

Article

## Origin of the Preferential Formation of Helicenes in Mallory Photocyclizations. Temperature as a Tool to Influence Reaction Regiochemistry.

Jacob Weber, and Edward L. Clennan

*J. Org. Chem.*, **Just Accepted Manuscript** • DOI: 10.1021/acs.joc.8b02671 • Publication Date (Web): 12 Dec 2018

Downloaded from <http://pubs.acs.org> on December 17, 2018

### Just Accepted

“Just Accepted” manuscripts have been peer-reviewed and accepted for publication. They are posted online prior to technical editing, formatting for publication and author proofing. The American Chemical Society provides “Just Accepted” as a service to the research community to expedite the dissemination of scientific material as soon as possible after acceptance. “Just Accepted” manuscripts appear in full in PDF format accompanied by an HTML abstract. “Just Accepted” manuscripts have been fully peer reviewed, but should not be considered the official version of record. They are citable by the Digital Object Identifier (DOI®). “Just Accepted” is an optional service offered to authors. Therefore, the “Just Accepted” Web site may not include all articles that will be published in the journal. After a manuscript is technically edited and formatted, it will be removed from the “Just Accepted” Web site and published as an ASAP article. Note that technical editing may introduce minor changes to the manuscript text and/or graphics which could affect content, and all legal disclaimers and ethical guidelines that apply to the journal pertain. ACS cannot be held responsible for errors or consequences arising from the use of information contained in these “Just Accepted” manuscripts.

1  
2  
3 **Origin of the Preferential Formation of Helicenes in Mallory**  
4 **Photocyclizations. Temperature as a Tool to Influence Reaction**  
5 **Regiochemistry.**  
6  
7

8 J. Weber, E. L. Clennan\*

9  
10 Department of Chemistry, University of Wyoming, Laramie WY, 82071

11  
12  
13 [clennane@uwyo.edu](mailto:clennane@uwyo.edu)  
14  
15  
16  
17

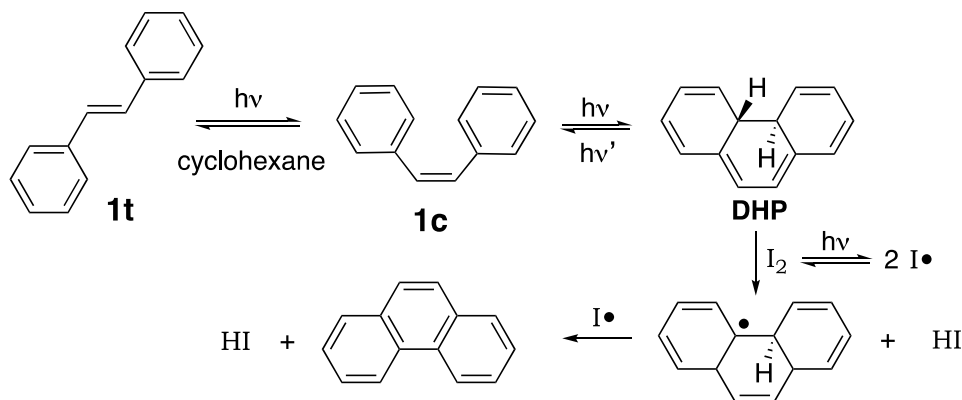
18  
19 **ABSTRACT**  
20

21 The regiochemistry of four bis-Mallory photocyclization substrates have been examined  
22 from experimental and computational perspectives. Formation of all three possible  
23 regioisomers was only observed in the reaction of one of the substrates. In the other three  
24 substrates only the two  $C_2$ -symmetric, but not the  $C_1$  product, were formed. In the three  
25 reactions that only formed two products the photocyclization temperature could be used to  
26 select for exclusive formation of one or the other regioisomer. The use of temperature to  
27 select between two regioisomers also worked in the photocyclization of the substrate that  
28 formed three products. However, no temperature was located for exclusive formation of  
29 the third component, one of the  $C_2$ -symmetric products, which always formed alongside  
30 either, one, or both of its regioisomers. B3LYP/6-311+G(2d,p) calculations were used to  
31 determine the energies of all of the dihydrophenanthrene (DHP), tetrahydrophenanthrene  
32 (THP), and mono-Mallory photocyclization intermediates. The oscillator strengths of the  
33 DHP precursors to the helicene products were a factor of 4.8 to 9.2 smaller than those of  
34 competitively formed DHPs. This observation suggests that establishment of a  
35  
36  
37  
38  
39  
40  
41  
42  
43  
44  
45  
46  
47  
48  
49  
50  
51  
52  
53  
54  
55  
56  
57  
58  
59  
60

1  
2  
3 photostationary state is responsible for the preferential formation of helicenes that has  
4  
5 been observed as a unique and useful feature of many Mallory photocyclizations.  
6

## 7 8 INTRODUCTION 9

10  
11  
12  
13 The Mallory photocyclization (Scheme 1) was first observed in 1934 and provided, at the  
14  
15 time, an unknown by-product during the photochemically initiated *cis-trans* isomerization of  
16  
17 stilbene,  $\mathbf{1t} \rightleftharpoons \mathbf{1c}$ .<sup>1</sup> This byproduct was subsequently identified by Parker and Spoerri<sup>2</sup> in 1950 as  
18  
19 phenanthrene. This reaction, although studied sporadically, was more or less dormant until  
20  
21 Mallory and coworkers<sup>3</sup> reported in 1962 its development into a preparatively useful oxidative  
22  
23 photocyclization by the use of I<sub>2</sub>, rather than O<sub>2</sub>, as the oxidant (Scheme 1). The key step in the  
24  
25 mechanism of the Mallory photocyclization is the widely recognized formation of a *trans*-  
26  
27 dihydrophenanthrene (DHP) intermediate<sup>4-7</sup> by an orbital symmetry allowed conrotatory  
28  
29 electrocyclic closure. (Scheme 1) This skeletal rearrangement in many diaryl-ethylenes is  
30  
31 photochromic and consequently has been utilized in the construction of a large number of  
32  
33 photoswitching devices.<sup>8</sup> The dihydrophenanthrene, DHP, however, in the Mallory  
34  
35 photocyclization is an intermediate, not an end-product, that is subsequently converted to the  
36  
37 phenanthrene end-product by abstraction of hydrogen and formation of HI.  
38  
39  
40  
41  
42  
43  
44  
45  
46  
47  
48  
49  
50  
51  
52  
53  
54  
55  
56  
57  
58  
59  
60



Scheme 1. The Mechanism for the Mallory Photocyclization of *trans*-Stilbene.

A Mallory photocyclization was used during the first synthesis of [7]helicene<sup>9</sup> and opened the door for decades of study of these fascinating polycyclic aromatic hydrocarbons (PAHs).<sup>10-13</sup> In addition, the importance of the Mallory photocyclization has subsequently been amply demonstrated by the publication of several reviews,<sup>14-19</sup> by the development of useful modifications,<sup>20-26</sup> and most recently by its use in the construction of carbon nanomaterials.<sup>27</sup> The sentence that appears in the elegant review of Morin, Daigel, and Desroche;<sup>27</sup> “The photochemical dehydrogenation, or Mallory reaction, is probably the most widely spread photochemical method for the preparation of carbon nanomaterials and PAHs.” is not hyperbole, and given the seemingly endless applications of PAHs (polycyclic aromatic hydrocarbons) underscores the value of further studies to understand the intimate details of this important reaction.

The mechanistic details of the photochemical interconversion of the *cis*-stilbene, **1c**, to the dihydrophenanthrene, DHP, (Scheme 1) step of the Mallory photocyclization has been extensively examined from both experimental<sup>28-30</sup> and theoretical<sup>31-34</sup> perspectives. A two-dimensional slice through the currently accepted potential energy surfaces (PES) for this reaction step is depicted in Figure 1. Upon irradiation of either **1c** or DHP an allowed transition to the corresponding Franck-Condon PES,  $FC_{\text{stilbene}}$  or  $FC_{\text{DHP}}$ , occurs. Rapid movement on the Franck-

Condon PES brings the vibrationally excited state into proximity to a conical intersection,  $CI_{FC}$ , where picosecond or sub-picosecond internal conversion to  $S_1$  takes place. Finally, both vibrationally excited states move on the  $S_1$  PES until they reach the critical conical intersection region,  $CI$ , where ultrafast deactivation forms either the *cis*-stilbene or the DHP on the  $S_0$  PES. The activation barrier,  $TS_1$  on the  $S_1$  PES, which was predicted theoretically, provides an explanation for both the observed temperature,<sup>35</sup> and wavelength,<sup>36</sup> dependence of the cycloreversion quantum yield for the DHP.

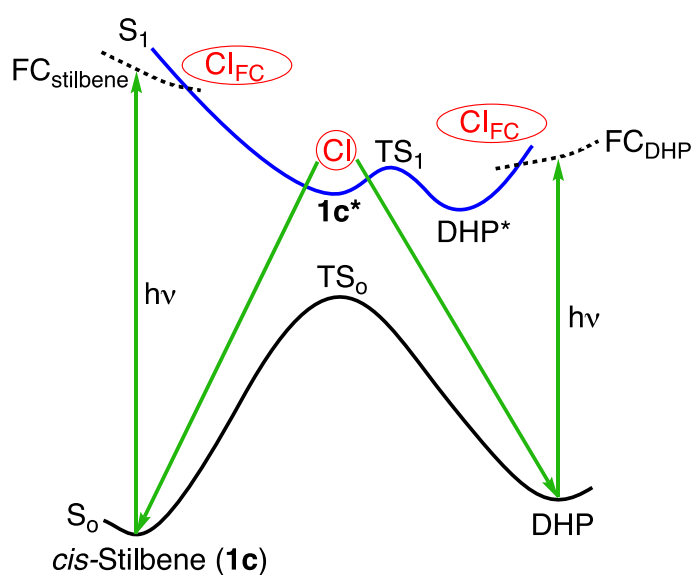
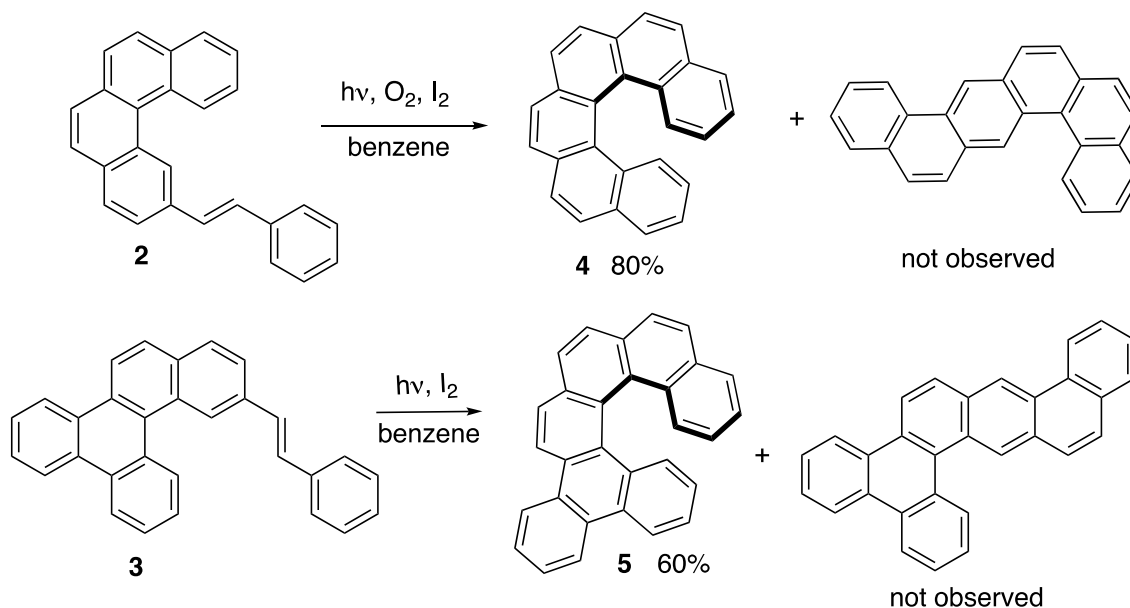


Figure 1. Potential Energy Surfaces Involved in the Reversible *cis*-Stilbene DHP Interconversion.

The detailed understanding of the *cis*-stilbene/DHP interconversion step of the Mallory photocyclization, however, stands in stark contrast to our fundamental lack of understanding, of perhaps the most unusual and distinguishing feature of the Mallory reaction, which is its propensity to form helicenes even when competing photocyclizations to form more thermodynamically stable, sterically less encumbered, planar PAHs are available. This phenomenon is illustrated with the reactions of **2**,<sup>37</sup> and **3**,<sup>16</sup> which exclusively produced

[6]helicene, **4**, and benzo[*b*]hexahelicene, **5**, without a trace of the alternative photocyclization products. (Scheme 2)



Scheme 2. Regioselectivity in Mallory Photocyclizations.

Laarhoven and coworkers<sup>38,39</sup> used the Coulson free valence numbers<sup>40</sup> to devise a set of rules to predict the regiochemical outcome of Mallory photocyclizations. These free valence numbers,  $\sum F_{rs}^*$ , are measures of the “residual affinity” for bond formation and are given by  $\sqrt{3} - \sum P$  for aromatic carbons where  $\sum P$  is the sum of the bond orders for the 3 bonds attached to the aromatic carbon in the excited state. According to the Laarhoven rules when the sum of the free valences of the two carbon atoms that form the new bond in the Mallory reaction are less than 1 (i.e.  $\sum F_{rs}^* < 1.0$ ) photocyclization does not occur. This reactivity parameter has been remarkably successful, however, other experimental parameters in addition to the identity of the substrate also influence the extent of regioselectivity including, the concentrations of the oxidant (e.g.  $I_2$ ,  $O_2$ ) and substrate, the identity of the solvent, and the temperature.<sup>41</sup> Despite the predictive power of the Laarhoven rules they do not provide a satisfying rationale or a

framework to control the unusual regiochemistry observed in many of these important photocyclizations.

In this manuscript we describe an experimental and computational study of the bis-Mallory photocyclizations of **6**, **7**, **8**, and **9** (Chart 1) focused on understanding the regioselectivity observed in these reactions. The experimental study reveals that the product regiochemistry in the reactions of **6** and **9** responds very differently to changes in experimental conditions and that the Mallory photocyclizations of **7** and **8** are intermediate in their behavior. The computational results are used to argue that the photostationary state established between competing DHPs plays an important role in these reactions. In addition, in those reactions that produce the helicene as the major product the photostationary state lies on the side of the DHP precursor to the helicene (DHP' Chart 1). These results provide valuable insight into Mallory photocyclizations that can be used to design new efficient photocyclization reactions.

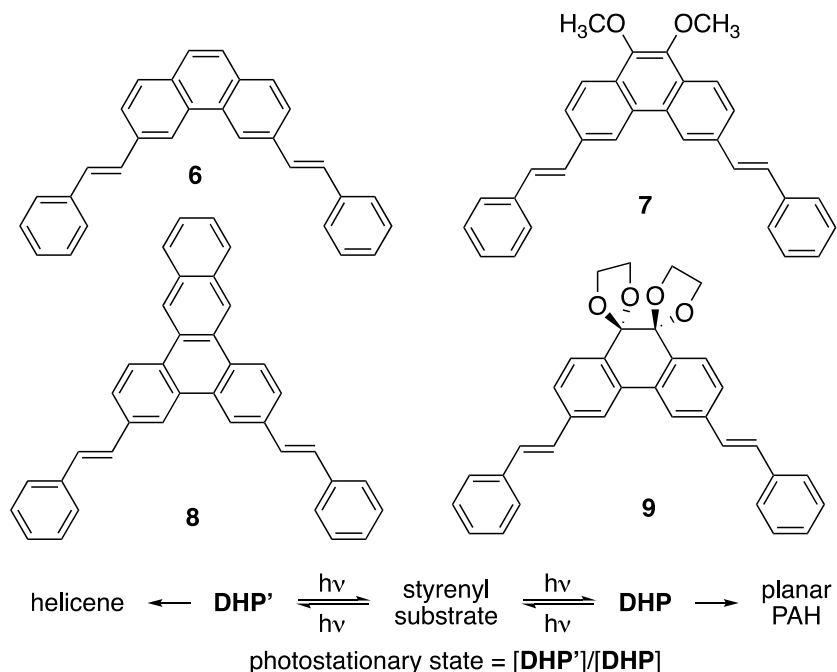
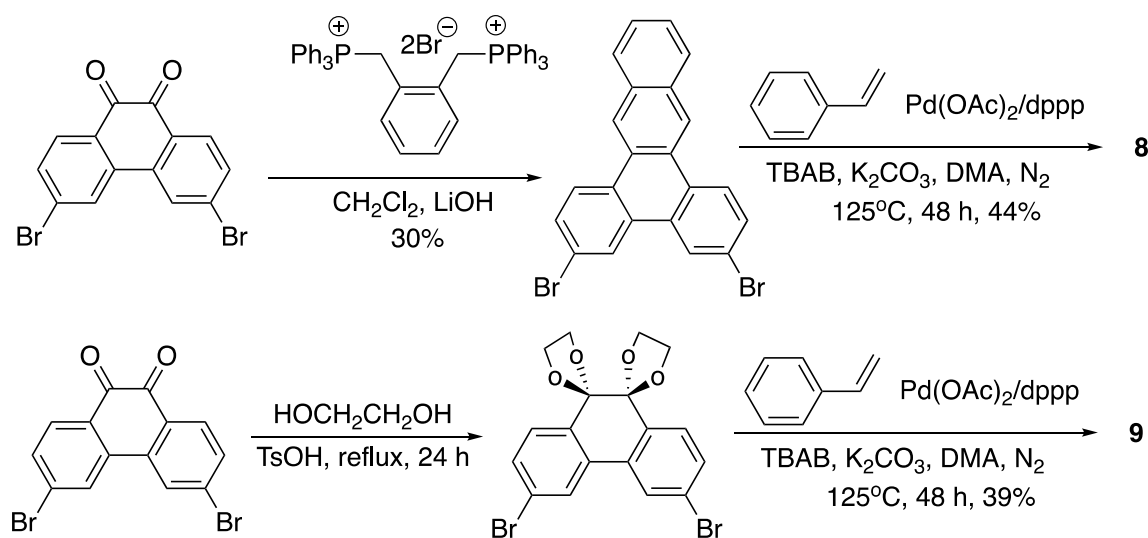


Chart 1.

## RESULTS

**Experimental Studies.** Bis-Mallory photocyclization substrates **8** and **9** were synthesized from 3,6-dibromophenanthrenequinone in straightforward two-step procedures as outlined in Scheme 3. The key steps were the Mizoroki-Heck reactions<sup>42</sup> which had previously been successfully used with 3,6-dibromophenanthrene and 3,6-dibromo-9,10-dimethoxyphenanthrene to make **6** and **7**, respectively.<sup>43</sup> Unfortunately, 3,6-bis-styrenylphenanthrene quinone, despite the fact that is readily accessible from a Mizoroki-Heck reaction, could not be used in this study. It is completely unreactive under our Mallory photocyclization conditions.



Scheme 3. Synthesis of bis-Mallory photocyclization substrates **8** and **9**.

The bis-Mallory photocyclizations were conducted by irradiation (600 W medium pressure mercury vapor lamp) of a 0.5 mM toluene solution of **6**, **7**, **8**, or **9** through the walls of a Pyrex vessel containing 1.1 mM iodine, and 25 mM propylene oxide.<sup>20</sup> At room temperature **9**

1  
2  
3 reacts to give a mixture of all three Mallory photocyclization products, the benzo[k]naphtho[1,2-  
4 a]tetraphene, **10d**, the [7]helicene, **11d**, and the dibenzo[c,m]pentaphene, **12d**. (Chart 2) The  
5  
6 benzo[k]naphtho[1,2-a]tetraphenes, **10a,b,c** however, were conspicuously absent from room  
7  
8 temperature irradiations of **6**, **7** and **8**. However, oxidation products **15b** and **15c** are formed in  
9  
10 approximately 40% yield during bis-Mallory photocyclizations of substrates, **7** and **8**,  
11  
12 respectively.<sup>44</sup> In addition, di-ester, **16**,<sup>45</sup> is also formed in approximately 5% yield in the  
13  
14 reactions of **7**. On the other hand, no oxidative cleavage of the styrenyl double bond was  
15  
16 observed in any of the phenanthrenyl substrates, **6-9**. This suggest that singlet oxygen formed by  
17  
18 self- sensitization is involved in these reactions since the singlet triplet energy gap is 5.4  
19  
20 kcal/mol smaller<sup>46</sup> and the intersystem crossing rate constant<sup>47</sup> to the triplet nearly 3 times larger  
21  
22 in the [5]helicene core<sup>48</sup> of **13b,c**, that is oxidatively cleaved to form **15b,c**, than in the  
23  
24 phenanthrene core of **6-9**, which are oxidatively inert. The formation of di-ester **16** can be  
25  
26 attributed to the well-established enhanced reactivity of singlet oxygen<sup>49,50</sup> with electron rich  
27  
28 enol ethers and to the even larger intersystem crossing rate constant of [7]helicene in comparison  
29  
30 to [5]helicene.<sup>47</sup> The amount of these oxidation products, however, can be substantially reduced  
31  
32 by exclusion of oxygen from the reaction mixtures. Products from further complications such as  
33  
34 hydrogen shifts in the dihydrophenanthrene, DHP, and *bis*-dihydrophenanthrene, *bis*-DHP,  
35  
36 intermediates, which have been observed in other systems were not detected in the reactions of  
37  
38  
39  
40  
41  
42  
43  
44  
45 **6-9**.<sup>16</sup>  
46  
47  
48  
49  
50  
51  
52  
53  
54  
55  
56  
57  
58  
59  
60

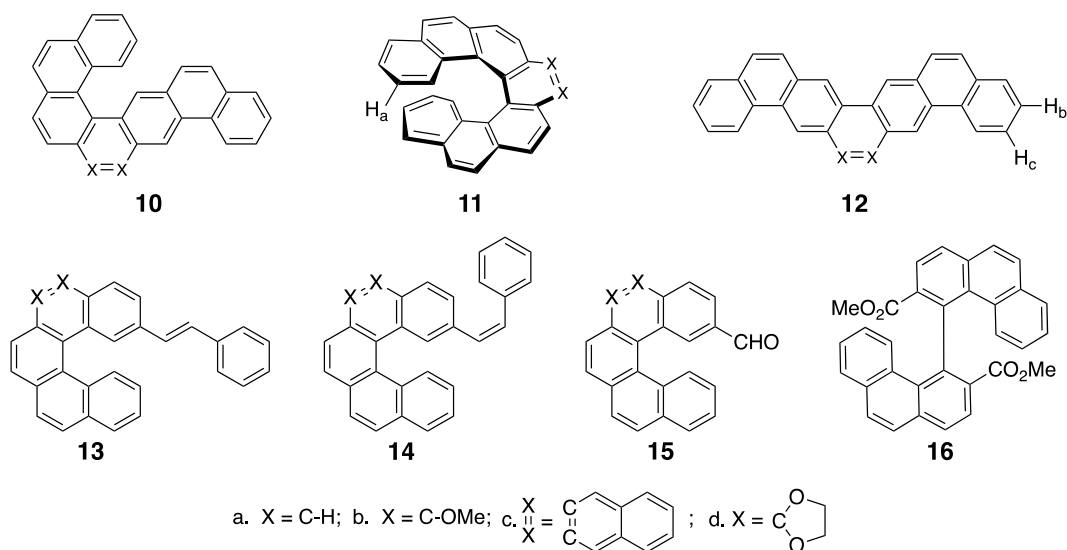


Chart 2.

These reactions were typically conducted overnight and the crude product mixtures analyzed by NMR spectroscopy. Products **11a**, **11b**, and **16** are known, and products **10d**, **11c**, **12c**, **12d**, **15b**, and **15c** were isolated, purified, and fully characterized by  $^1\text{H}$  and  $^{13}\text{C}$  NMR spectroscopy (with the exception of **12c** whose limited solubility precluded collection of its  $^{13}\text{C}$  NMR spectrum), and by high-resolution mass spectrometry. Diagnostic peaks in the NMR spectra of these conclusively identified products were then used to identify their homologues (**11d**, **12a**, **12b**, and **12c**) formed in the other Mallory photocyclization reactions. Stacked comparator  $^1\text{H}$  NMR plots used in this analysis are provided in the Supporting Information for the **11**, and **12** homologous series. A diagnostic ddd for proton  $\text{H}_2$  (Chart 2) showed up in the **11** comparator spectra at approximately 6.4 ppm in all of the [7]helicenes **11a**, **b**, **c**, and **d**. This proton was upfield of all other peaks in the reaction mixtures because it is located in the shielding cone of the terminal ring on the other end of the helicene. The dibenzo[c,m]pentaphenes, **12**, were also easily identified because Mallory photocyclization conditions (vide infra) are available where these compounds are the major or exclusive product of the reaction. Their most upfield peaks, between 7.6 and 7.7 ppm are also ddd's and are

readily assigned to H<sub>4</sub> and H<sub>5</sub>. The *cis*- and *trans*-3-strenyl[5]helicenes, **13** and **14**, were identified as fleeting intermediates in the crude reaction mixtures by their characteristic doublet-of-doublets for the styrenyl double bond. (See Supporting information)

The product compositions at approximately 40°C during Mallory photocyclizations of **6-9** as a function of irradiation time are given in Figure 2. The mono-Mallory products **13** and **14** form rapidly followed by slower formation of the [7]helicenes **11**. In addition, the yields of the [7]helicenes decrease in the order **6** > **7** > **8** > **9**. The photocyclization of **9** (Figure 2) was complete in approximately 5 h in comparison to the 10-12 hours of irradiation needed to produce the final products in the reactions of **6**, **7**, and **8**. The photocyclization of **9** also produced **10d** under these conditions as the dominant product in approximately 85% yield. In contrast, **10a,b,c** were not observed at any point during the photocyclizations of **6**, **7**, or **8**.

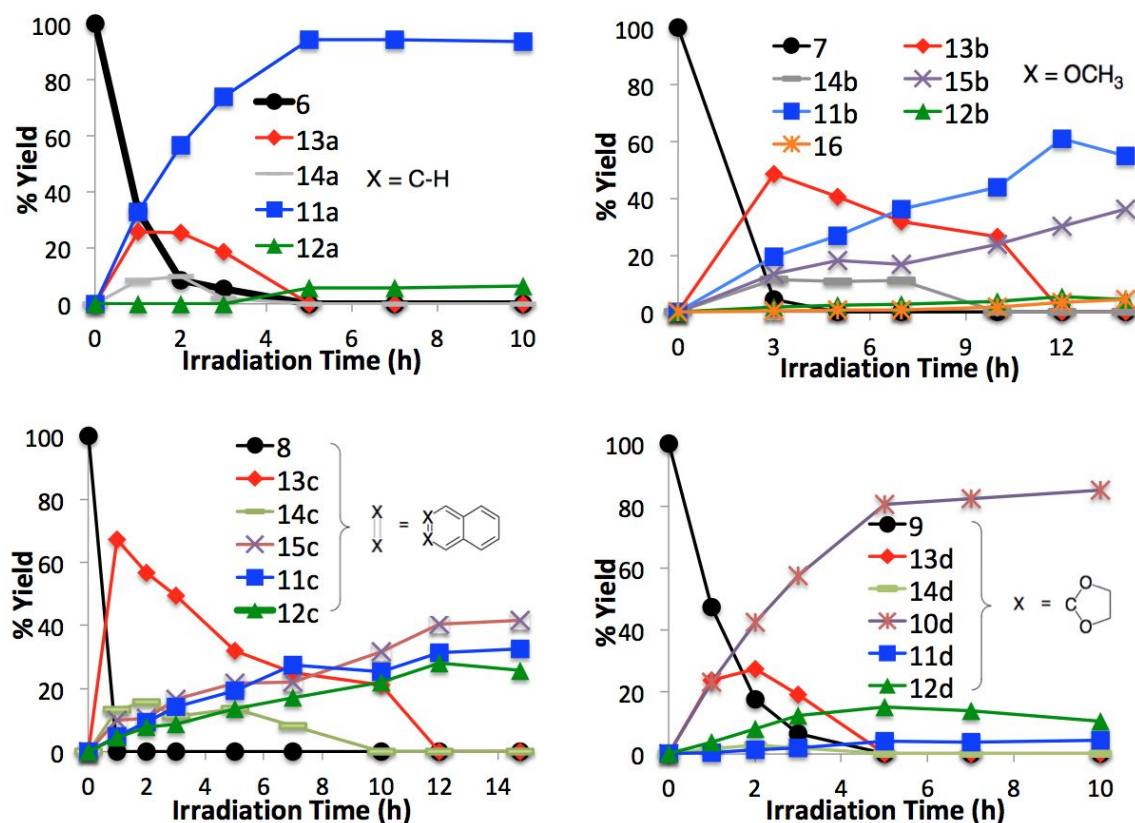


Figure 2. Reaction Compositions as a Function of Time at 40°C.

The effect of temperature on the Mallory photocyclizations was examined by running each of the reactions in a pyrex vessel submerged in an appropriate temperature-controlled bath. The products were then analyzed by NMR spectroscopy and their relative yields plotted versus temperature as depicted in Figure 3. The [7]helicenes, **11a**, **11b**, and **11c** were the exclusive products in the reactions of **6**, **7**, and **8** at low temperatures ( $< 0^{\circ}\text{C}$ ). On the other hand, the [7]helicene, **11d**, is observed, but its % yield peaks at approximately  $0^{\circ}\text{C}$  and never becomes the major product at any temperature between  $-30^{\circ}\text{C}$  and  $+150^{\circ}\text{C}$ . In all four Mallory photocyclizations the thermodynamically most stable product (vide infra), the planar dibenzo[*c,m*]pentaphene, **12**, is the dominant product at high temperature.

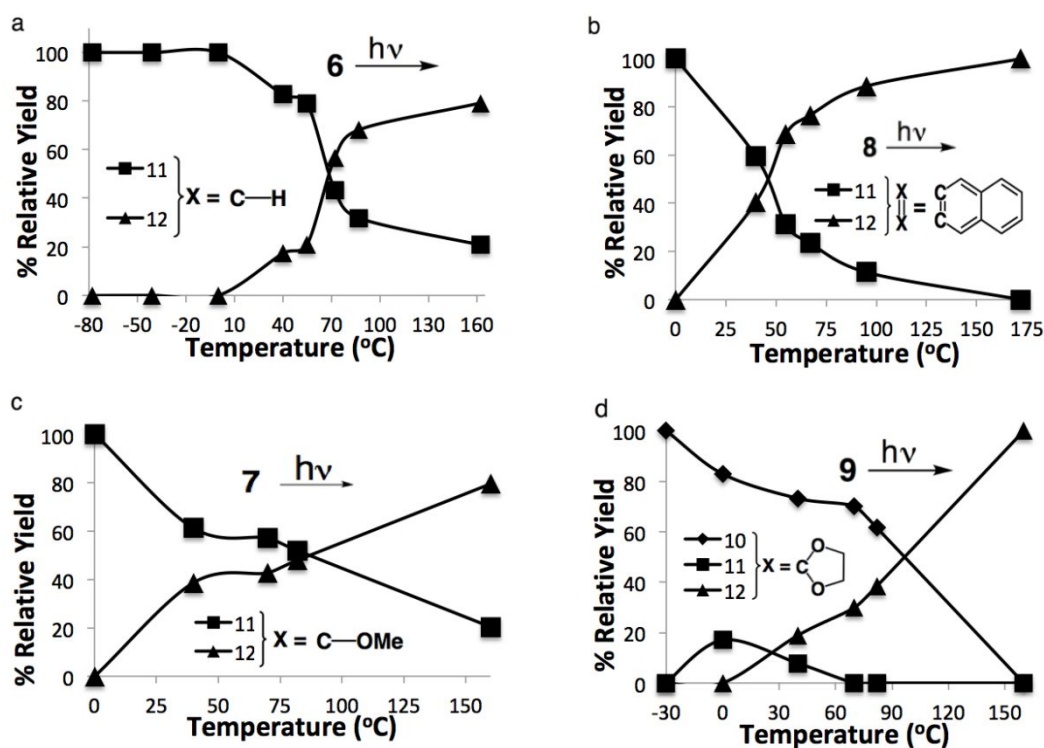


Figure 3. Relative product composition as a function of temperature for the Mallory photocyclizations of **6**, **7**, **8**, and **9**. All reactions were run under an atmosphere of air, however, the oxygenated products are not included in the plots.

**Computational Studies.** The mechanisms of the bis-Mallory photocyclizations of **6-9** are considerably more complex than the simple photocyclization of *cis*-stilbene shown in Scheme 1. The bis-Mallory substrates undergo two photocyclizations and each photocyclization can occur at two different sites on the phenanthrene core to give two different DHPs. This leads to eleven different possible closed shell intermediates on these very complicated reaction surfaces in addition to the three possible products, **10**, **11**, and **12**. The structures of all the potential intermediates are depicted in Chart 3.

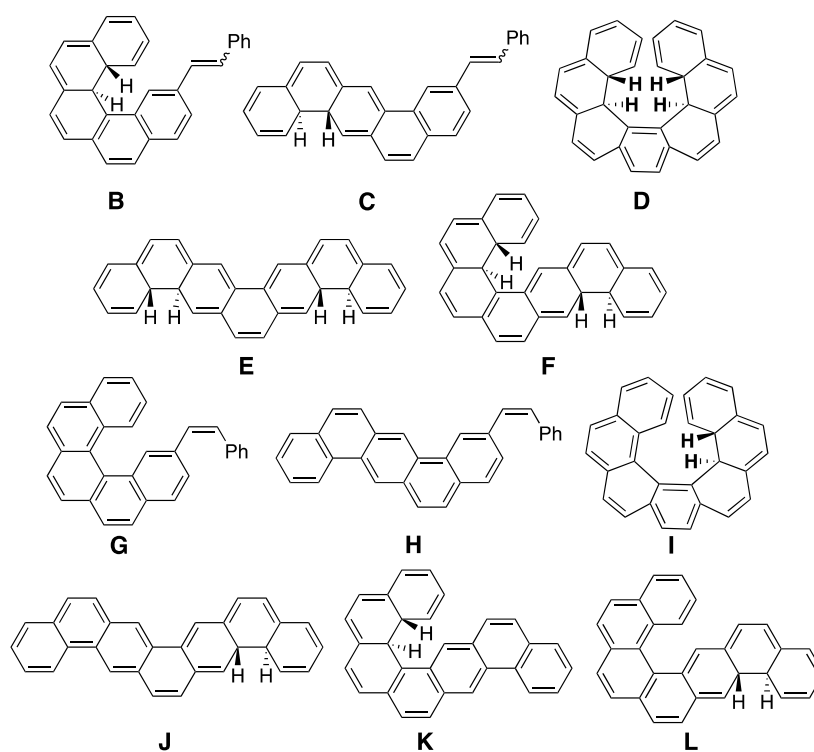
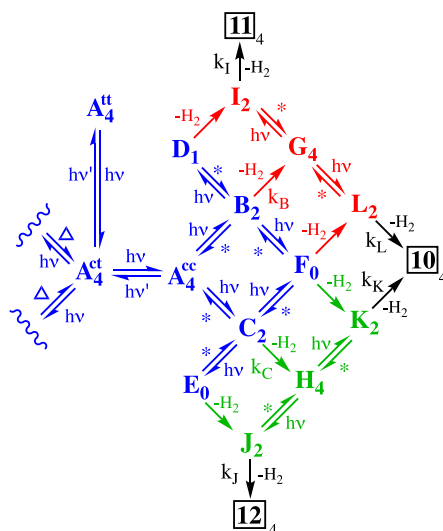


Chart 3. Potential intermediates in the Mallory bis-photocyclization of **6**.

In order to facilitate the consideration of the computational results and the upcoming consideration of potential mechanisms in the discussion section of the manuscript, these intermediates are organized using the interconversion diagram shown in Scheme 4. However, it is important to recognize that this complicated interconversion diagram is itself a simplification of the actual potential energy surface. Both diastereomers of the DHP regioisomers depicted in

1  
2  
3 Chart 3, which are generated by competing clockwise and counterclockwise ring closures, are  
4 not explicitly included in the interconversion diagram. This is not a serious omission. A single  
5 diastereomer thermodynamically dominates in most cases (Table 1) but even in those cases  
6 where two stereoisomers might be simultaneously present (e.g.  $\mathbf{E}_{\text{tet}}$  and  $\mathbf{E}_{\text{ttt}}$  in Table 1; see  
7 Supporting Information for detailed structural information) it will not change the mechanistic  
8 conclusions discussed below. Consequently, all the Tables in this manuscript, except Table 1,  
9 contain only those values calculated using the thermodynamic data for the most stable  
10 diastereomer of each of the DHP regioisomers shown in Chart 3.  
11  
12  
13  
14  
15  
16  
17  
18  
19  
20  
21

22 The  $\mathbf{A}$ 's in the interconversion diagram represent the *cis-cis* (cc), *cis-trans* (ct), and *trans-*  
23 *trans* (tt) isomers of the bis-styrenyl starting materials, **6-9**, and the subscripts represent the total  
24 number of Clar sextets<sup>51</sup> (i.e. the number of six membered rings with a localized aromatic  
25  $6\pi$  cyclic array of electrons). The remaining letters (See Chart 3 and Scheme 4) represent either  
26 dihydrophenanthrenes, **B**, **C**, **I**, **J**, **K**, and **L**, each with 2 Clar sextets, or *bis-*  
27 dihydrophenanthrenes, **D**, **E**, and **F**, with 1, 0, and 0 Clar sextets, respectively, or mono-Mallory  
28 photocyclized intermediates, **G** and **H**, containing 4 Clar sextets. To the left, emanating from  $\mathbf{A}^{\text{ct}}$   
29 is an identical interconversion diagram differing only from the one on the right by the *trans-*  
30 configuration of the styrenyl double bond in intermediates **B**, **C**, **G** and **H**. The mechanistic  
31 conclusions that can be deduced from either wing of the interconversion diagram are identical so  
32 we will use the expanded right hand wing for the remaining discussion. Intermediates in  
33 different colored regions of the diagram are not interconvertible, either thermally or  
34 photochemically, because it would require reversible loss of  $\text{H}_2$ , which is highly improbable.  
35 The \*'s in the diagram are for microscopic steps that can occur either thermally by a stepwise, or  
36 concertedly by a controtatory photochemically allowed process.  
37  
38  
39  
40  
41  
42  
43  
44  
45  
46  
47  
48  
49  
50  
51  
52  
53  
54  
55  
56  
57  
58  
59  
60



Scheme 4. Interconversion diagram for intermediates in the Bis-Mallory Photocyclizations of **6**, **7**, **8**, and **9**. \* hv or heat; cc *cis-cis* and ct *cis-trans*; subscripts on all numerical and letter compound designations refer to its number of Clar sextets.

DFT based-methods with large basis sets have been shown to perform well in thermochemical studies of large polyaromatic hydrocarbons and in studies of delocalized radicals.<sup>52</sup> Consequently, we used the B3LYP/6-311+G(2d,p) computational method to optimize and determine the energies of all the diastereomers for the regioisomeric intermediates located on the right hand side of Scheme 4, including the products **10**, **11**, and **12**. The energies are given in Table 1 and the optimized geometries are provided in the supporting information.

The stabilities of the  $C_{30}H_{22}$  isomers (for **6**) in the blue region and the  $C_{30}H_{20}$  isomers in the green/red regions of Scheme 4 decrease with the decreasing number of Clar sextets (blue:  $A_4^{cc} > B_2 \cong C_2 > E_0 \cong F_0$  and green/red:  $H_4 \cong G_4 > I_2 \cong J_2 \cong K_2 \cong L_2$ ). Superimposed on these primarily aromaticity driven stability sequences there is also a strain/steric contribution. In the reactions of **6** and **7** this internal strain raises the energy of the most stable isomer of the tetrahydro[7]helicene **D** with one Clar sextet above that of both **E** and **F** with zero Clar sextets. In the reactions of all the bis-Mallory substrates, **6-9**, the embedded [5]helical structure in **F**

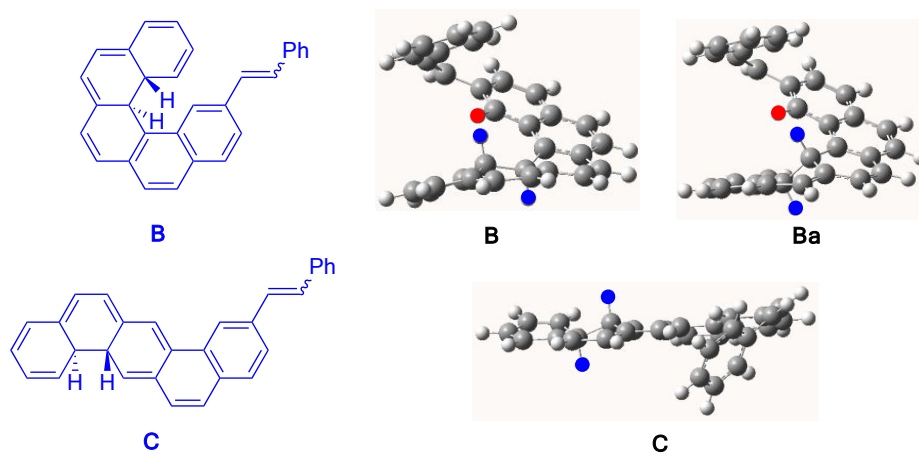
raises its energy by 6 or more kcal/mol above that of **E** despite the fact that both contain the same number of Clar sextets (zero). The internal strain energy imparted by the helical architecture, and the greater strain imparted by the [7]- relative to the [5]helical architecture, is also expressed in the relative energies of the final bis-Mallory products, (**11** > **10** > **12**) all of which can be drawn with 4 Clar sextets. (Table 1)

Table 1. Relative Free Energies<sup>a</sup> of bis-Mallory Reaction Stationary Points with Zero Negative Frequencies.<sup>a</sup>

<b>C<sub>x</sub>H<sub>y+4</sub> (Blue Region)<sup>b</sup> Bis-Mallory Reaction Intermediates<sup>c</sup></b>				
	<b>6(parent)</b>	<b>7(di-MeO)</b>	<b>8(Naphtho)</b>	<b>9(Bis-Ketal)</b>
<b>A</b>	0	0	0	0
<b>B</b>	49.8	50.7	52.8	52.4
<b>Ba</b>	44.2	44.8	46.0	48.1
<b>C</b>	46.1	45.8	42.8	39.1
<b>Diioi</b>	101.7	102.8	105.5	107.4
<b>Doiio</b>	84.3	85.0	90.6	96.7
<b>Doioi</b>	89.9	90.7	97.0	101.3
<b>Etct</b>	85.9	85.6	84.1	78.7
<b>Ettt</b>	85.2	85.8	83.4	78.1
<b>Ftct</b>	93.7	93.9	89.4	85.2
<b>Ftcta</b>	97.1	97.5	93.7	88.7
<b>Fttt</b>	99.2	99.4	96.1	90.5
<b>Fttta</b>	92.3	92.1	89.0	85.5
<b>C<sub>x</sub>H<sub>y+2</sub> (Red/Green Region)<sup>b</sup> Bis-Mallory Reaction Intermediates<sup>c</sup></b>				
	<b>6(parent)</b>	<b>7(di-MeO)</b>	<b>8(Naphtho)</b>	<b>9(Bis-Ketal)</b>
<b>G</b>	13.4	13.2	13.7	12.4
<b>H</b>	0	0	0	0
<b>I</b>	60.9	61.7	63.7	63.4
<b>Ia</b>	57.4	58.2	60.8	62.2
<b>J</b>	45.0	44.5	42.9	39.5
<b>K</b>	50.4	51.2	53.2	52.0
<b>Ka</b>	44.7	45.0	46.4	47.8
<b>L</b>	61.1	61.1	57.8	52.0
<b>La</b>	58.0	58.0	55.3	50.6
<b>C<sub>x</sub>H<sub>y</sub> (Black)<sup>b</sup> Final Reaction Products<sup>c</sup></b>				
<b>10</b>	13.2	13.7	13.3	11.9
<b>11</b>	24.2	24.4	25.5	23.4
<b>12</b>	0	0	0	0

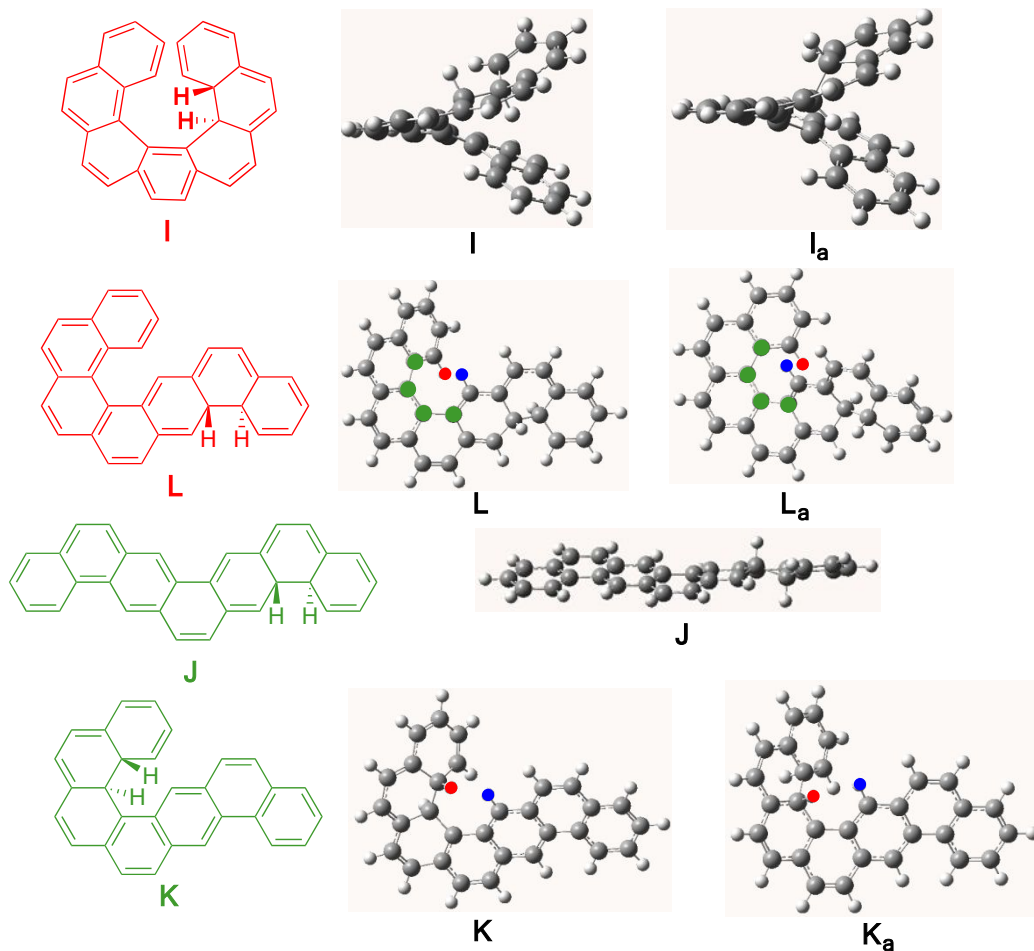
a. B3LYP/6-311+G(2d,p) sum of electronic and thermal Free Energies in kcal/mol. b. See Scheme 4 for region colors. c. X = number of carbons in **6-9**; Y = number of hydrogens in the final reaction products, **10-12**, of bis-Mallory photocyclization/oxidation of **6-9**.

The dihydrophenanthrenes, **B** and **C**, are key intermediates in the blue region (Scheme 4) of the bis-Mallory photocyclizations of **6-9**. The most stable isomers of the *bis*-dihydrophenanthrenes, **D**, **E**, and **F**, (Table 1) formed in the blue region are approximately  $42.6 \pm 6.0$ ,  $36.6 \pm 6.6$ , and  $43.2 \pm 5.8$  kcal/mol higher in energy than the least stable dihydrophenanthrene and are unlikely to be involved in the reactions. The B3LYP/6-311+G(2d,p) optimized structures of **B** and **C** formed in the photocyclization of **6** are shown in Scheme 5 and have the *trans*-configuration of the hydrogens at the dihydrophenanthrene ring closure junctions as dictated by the allowed conrotatory closure. The two conrotatory closures in **B** lead to diastereomers **B** and **Ba**. Diastereomer **B** (PRR/MSS configuration) is 5.6 kcal/mol less stable than diastereomer **Ba** (PSS/MRR configuration) as a result of the 0.36 Å closer approach ( $1.765 \text{ \AA}$  vs.  $2.128 \text{ \AA}$ ) of the blue and the red hydrogens (Scheme 5). The two conrotatory closures to form the **C** intermediates are very close in energy at the B3LYP/6-31G(d) computational level ( $\Delta\Delta G^\circ(\text{RB3LYP}) = 0.4 \text{ kcal/mol}$ ) so only the most stable diastereomer was optimized at the higher B3LYP/6-311+G(2d,p) computation level and included in Table 1 and Scheme 5.



Scheme 5. Structures of the dihydrophenanthrene intermediates, **B** and **C**, formed in the bis-Mallory photocyclization of **6**.

1  
2  
3  
4 The key dihydrophenanthrene intermediates in the red and green regions (Scheme 4) of  
5 the interconversion diagram, **I**, **J**, **K**, and **L**, which are formed in the photocyclization of **6**, are  
6 shown in Scheme 6. (P)-18a(S), 18b(S)-Dihydro[7]helicene **I<sub>a</sub>** is 3.5 kcal/mol more stable than  
7 its isomer (P)-18a(R), 18b(R)-dihydro[7]helicene **I**. Isomer **I<sub>a</sub>** is also likely to form faster  
8 because it is formed by photocyclization on the least hindered face of the [5]helicene  
9 intermediate, **G**. (P)-Naphtho[1,2,b]-14a(R), 14b(R)-dihydro[5]helicene, **K**, is significantly  
10 destabilized, by 5.7 kcal/mol, relative to (P)-naphtho[1,2,b]-14a(S), 14b(S)-dihydro[5]helicene,  
11 **K<sub>a</sub>**, by the energetically costly 1.78 Å through space H<sub>1</sub>-H<sub>14a</sub> distance, which is increased to a  
12 sterically more tolerable 2.23 Å H<sub>1</sub>-H<sub>14b</sub> closest approach distance in **K<sub>a</sub>** (H<sub>1</sub> blue atom and  
13 H<sub>14a,14b</sub> red atoms in Scheme 6). (P)-1(R), 8a(S)-dihydronaphtho[1,2,b]-[5]helicene, **L**, is 3.1  
14 kcal/mol less stable than its isomer (P)-1(S), 8a(R)-dihydronaphtho[1,2,b]-[5]helicene, **L<sub>a</sub>**, due  
15 in part to the shorter H<sub>1</sub>-H<sub>14</sub> (blue and red atoms in Scheme 6) through space distance (2.60 Å in  
16 **L** and 2.82 Å in **L<sub>a</sub>**) and by the increased strain in the helical section of the intermediate as  
17 revealed by a 3.1° increase in the C<sub>14a</sub>-C<sub>14b</sub>-C<sub>14c</sub>-C<sub>14d</sub> internal dihedral angle (green atoms in **L**  
18 and **L<sub>a</sub>** in Scheme 6).  
19  
20  
21  
22  
23  
24  
25  
26  
27  
28  
29  
30  
31  
32  
33  
34  
35  
36  
37  
38  
39  
40  
41  
42  
43  
44  
45  
46  
47  
48  
49  
50  
51  
52  
53  
54  
55  
56  
57  
58  
59  
60



Scheme 6. Structures of the dihydrophenanthrene intermediates, **I**, **L**, **J**, and **K**, formed in the bis-Mallory photocyclization of **6**.

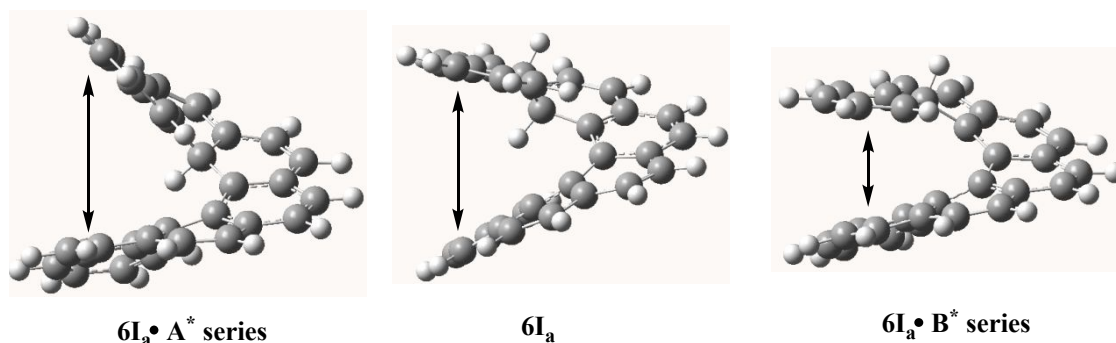
The DHPs shown in Schemes 5 and 6 are subsequently oxidized by stepwise removal of two hydrogen atoms with photochemically generated iodine atoms. Aromatic resonance energy is recovered as a result of the second hydrogen abstraction and as a result the first hydrogen abstraction is likely to be the rate determining step for formation of the fully polyaromatic hydrocarbon product. The initial hydrogen abstraction can occur from the terminal or internal ring of the DHP leading to two different radicals, the  $A^*$  and  $B^*$  series, respectively. The relative energies of these radicals generated by hydrogen abstraction from **B<sub>a</sub>**, **C**, **I<sub>a</sub>**, **J**, **K<sub>a</sub>**, and **L<sub>a</sub>** in the reactions of **6** and **9** are given in Table 2. Hydrogen abstraction is prohibitively favored

( $\Delta\Delta G^0 \geq 14.4 \text{ kcal/mol}$ ) from the terminal ring to give the  $A^*$  series when the DHP is part of the helical domain (i.e.  $\mathbf{B}_a$ ,  $\mathbf{I}_a$ , and  $\mathbf{K}_a$ ). On the other hand, the energies of the  $A^*$  and  $B^*$  series radicals, formed by hydrogen abstraction from the DHPs that reside in the acene domain (i.e.  $\mathbf{C}$ ,  $\mathbf{J}$ , and  $\mathbf{L}_a$ ), are nearly equal. Formation of the  $A^*$  series radicals from the helical embedded DHPs open up the jaws of the helicene decreasing steric interactions while formation of the  $B^*$  series radicals closes the jaws and increases the intra-helicene steric interactions (Scheme 7). The formation of the  $A^*$  series radicals in the helical domain embedded DHPs are also likely kinetically preferred since the hydrogen on the terminal ring is on the periphery of the helicene while the internal hydrogen is buried in the jaws of the helical clef. (See  $\mathbf{B}_a$  in Scheme 5 and the supporting information).

Table 2. Relative Energies of Radicals formed in Mallory Cyclizations of **6** and **9**.<sup>a,b</sup>

	<b>6</b>		<b>9</b> <sup>c</sup>	
	$A^*$	$B^*$	$A^*$	$B^*$
$\mathbf{B}_a$	1.0	17.6	5.4	15.1
$\mathbf{C}$	1.4	0	0	2.6
$\mathbf{I}_a$	14.2	28.6	19.8	27.6
$\mathbf{J}$	0.6	0	0	2.83
$\mathbf{K}_a$	1.0	16.4	5.2	15.2
$\mathbf{L}_a$	12.1	12.6	11.3	14.9

- a. Relative B3LPY/6-311+G(2d,p) sum of electronic and thermal Free Energies in kcal/mol for the radicals generated from the most stable DHP diastereomer (See Table 1). b.  $A^*$  – radical formed by hydrogen abstraction from the terminal ring of DHP;  $B^*$  – radical formed by hydrogen abstraction from internal ring of DHP. c. Calculated at the B3LYP/6-31G(d) level.



Scheme 7. Steric Interactions in  $6I_a$  in comparison to those observed in the  $A^*$  and  $B^*$  series hydrogen abstraction products (radicals)

The UV-Vis spectra of the DHPs were calculated using the TD-DFT/6-311+G(2d,p) computational model. The lowest energy transitions are given in Table 3 along with their oscillator strengths. The DHPs (i.e.  $B_a$  and  $C$ ,  $I_a$  and  $L_a$ , and  $K_a$  and  $J$ ) in the same colored region of Scheme 4 are thermally and photochemically interconvertible and are placed in the same rows of Table 3 for comparison. The HOMO-LUMO determinant in all cases was the  $\geq 99\%$  contributor to the excited-state wavefunction as determined by taking two times the square of the coefficient for the configuration interaction expansion. The absorbance maxima are all between 580 and 750 nm consistent with the transient formation of a colored intermediate noted in many Mallory photocyclizations.<sup>53</sup> For example, the bathochromic absorption maxima for DHPs **17**, **18**, and **19** (Chart 4) are reported at 603 nm, 448 nm, and 530 nm, respectively, with extinction coefficients of approximately 10,000-12,000  $M^{-1}cm^{-1}$ .<sup>54</sup> The oscillator strengths (f) for the DHPs embedded in helical domains (column 3) were 5 to approximately 9 times smaller than those embedded in acene domains (column 6, Table 3).

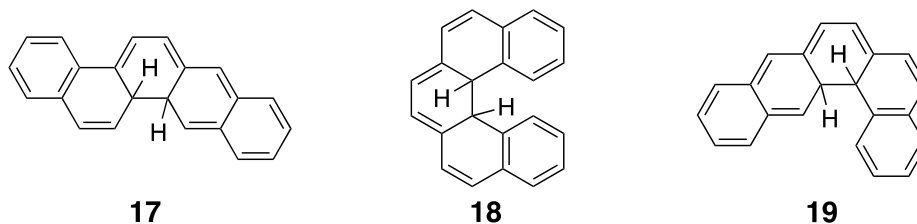


Chart 4

Table 3. Wavelength Maxima and Oscillator Strengths of Low Energy DHP UV/Vis Absorbances.<sup>a</sup>

	$\lambda_{\text{MAX}}^{\text{b}}$	$f^{\text{c}}$		$\lambda_{\text{MAX}}^{\text{b}}$	$f^{\text{c}}$
<b>6</b>					
<b>B<sub>a</sub></b>	683	0.0622	<b>C</b>	663	0.3135
<b>I<sub>a</sub></b>	689	0.0628	<b>L<sub>a</sub></b>	704	0.3325
<b>K<sub>a</sub></b>	727	0.0527	<b>J</b>	662	0.4857
<b>7</b>					
<b>B<sub>a</sub></b>	688	0.0619	<b>C</b>	670	0.2946
<b>I<sub>a</sub></b>	696	0.0631	<b>L<sub>a</sub></b>	713	0.3154
<b>K<sub>a</sub></b>	732	0.0514	<b>J</b>	670	0.4500
<b>8</b>					
<b>B<sub>a</sub></b>	717	0.0617	<b>C</b>	624	0.4144
<b>I<sub>a</sub></b>	730	0.0629	<b>L<sub>a</sub></b>	667	0.4358
<b>K<sub>a</sub></b>	743	0.0683	<b>J</b>	630	0.5821
<b>9</b>					
<b>B<sub>a</sub></b>	713	0.0877	<b>C</b>	585	0.4764
<b>I<sub>a</sub></b>	720	0.0888	<b>L<sub>a</sub></b>	601	0.5019
<b>K<sub>a</sub></b>	730	0.1019	<b>J</b>	607	0.6746

a. Calculated at the TD-DFT/6-311+G(2d,p) level in toluene. b. Wavelength of lowest energy transition.  
c. Oscillator strength.

## DISCUSSION

As evident from examination of the interconversion diagram in Scheme 4 the yields of the three products formed in the bis-Mallory photocyclizations are sensitive functions of the concentrations of the DHPs (**[B]**, **[I]**, etc.) and of the rate constants for hydrogen abstraction,  $k_{\text{DHP}}$  (e.g.  $k_{\text{I}}$ ,  $k_{\text{B}}$ , etc.). This is expressed mathematically in Eqns. 1, 2, and 3. The yield of **11** for example is the product of the fraction of the precursor **B** formed in the blue region  $\phi_{\text{B}}$  and the fraction of **I** formed in the red region  $\phi_{\text{I}}$ . The yield of **10** on the other hand has two terms since it can be formed in both the green and red region of Scheme 4.

$$\% \mathbf{10} = [\phi_L \phi_B + \phi_K \phi_C] \times 100 \quad 1$$

$$\% \mathbf{11} = \phi_I \phi_B = \left( \frac{k_I[I]}{k_I[I] + k_L[L]} \right) \left( \frac{k_B[B]}{k_B[B] + k_C[C]} \right) \times 100 \quad 2$$

$$\% \mathbf{12} = \phi_J \phi_C = \left( \frac{k_J[J]}{k_J[J] + k_K[K]} \right) \left( \frac{k_C[C]}{k_B[B] + k_C[C]} \right) \times 100 \quad 3$$

Several experimental and structural variables can influence the concentrations of the DHPs and the rate constants of hydrogen abstraction,  $k_{\text{DHP}}$ , whose magnitudes dictate product formation (Eqns. 1, 2, and 3). These include: (1) The position of the photostationary state established between the two competing DHPs; (2) the relative stability of the competing DHPs; (3) the relative stabilities of DHP radicals ( $A^*$ ) produced during hydrogen abstraction from the competing DHPs; and (4) experimental variables such as reaction temperatures.

(1) The photostationary states established between the two competing DHPs in the mutually inaccessible blue, red, and green regions of Scheme 4 are given by equations **4a**, **4b**, and **4c**, respectively. These equations are analogous to the equation for the photostationary state reached upon irradiation of *cis*- and *trans*-alkenes<sup>55</sup> but differs because it is the product of two photostationary equilibria, for example  $\mathbf{L} \rightleftharpoons \mathbf{G}$  and  $\mathbf{G} \rightleftharpoons \mathbf{I}$  in the red region of Scheme 4. The ratio, of the extinction coefficients,  $\epsilon_L / \epsilon_I$ , at the  $\lambda_{\text{MAX}}$  of the HOMO  $\rightarrow$  LUMO absorption peaks for the DHPs shown in Table 3, are proportional to the ratio of oscillator strengths<sup>56</sup> (Table 3) when the band widths are the same. This relationship also implies that the ratio of DHP concentrations will change with changing irradiation wavelength. This is consistent with the observation of Fisher and coworkers<sup>53</sup> who observed a strong wavelength dependence on the

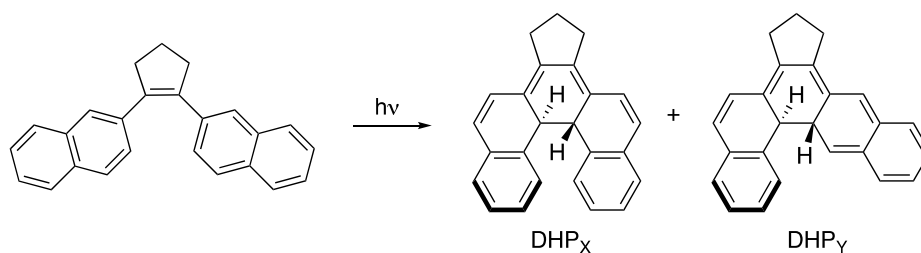
ratio of DHP<sub>X</sub>/DHP<sub>Y</sub> during the Mallory photocyclization of 1,2-di-(2-naphthyl)cyclopentene.

(Scheme 8)

$$\frac{[B]}{[C]} = \frac{\varepsilon_C}{\varepsilon_B} \cdot \frac{(\phi_{A \rightarrow B})(\phi_{C \rightarrow A})}{(\phi_{B \rightarrow A})(\phi_{A \rightarrow C})} \quad \mathbf{4a}$$

$$\frac{[I]}{[L]} = \frac{\varepsilon_L}{\varepsilon_I} \cdot \frac{(\phi_{G \rightarrow I})(\phi_{L \rightarrow G})}{(\phi_{I \rightarrow G})(\phi_{G \rightarrow L})} \quad \mathbf{4b}$$

$$\frac{[K]}{[J]} = \frac{\varepsilon_J}{\varepsilon_K} \cdot \frac{(\phi_{H \rightarrow K})(\phi_{J \rightarrow H})}{(\phi_{K \rightarrow H})(\phi_{H \rightarrow J})} \quad \mathbf{4c}$$



Scheme 8. DHP diastereomers formed during Mallory photocyclization of 1,2-di-(2-naphthyl)cyclopentene.

(2) The relative stabilities of the competing DHPs in the blue (**B<sub>a</sub>-C**), red (**I<sub>a</sub>-L<sub>a</sub>**), and green (**K<sub>a</sub>-J**) regions of the mechanism shown in Scheme 4 are compared in terms of both their free energies in Table 1 and enthalpies in Table 4. This data reveals that the DHPs in the reactions of **6** and **7** that are embedded in the helical domain, **B<sub>a</sub>**, **I<sub>a</sub>**, and **K<sub>a</sub>**, and are the precursors for formation of a helical product, are equal or perhaps slightly more stable than the DHPs embedded in the acene domain, **C**, **L<sub>a</sub>**, and **J**. (Columns 2 and 3 in Table 4). On the other hand Mallory substrates **8** and **9** exhibit the opposite behavior with their acene-embedded DHPs, **C**, **L<sub>a</sub>**, and **J**, more stable than their helicene-embedded DHPs, **B<sub>a</sub>**, **I<sub>a</sub>**, and **K<sub>a</sub>**. This stability preference for **C**, **L<sub>a</sub>**, and **J** in **9** is especially large (7.0-10.1 kcal/mol) and essentially precludes all but a trace of **B<sub>a</sub>**, **I<sub>a</sub>**, and **K<sub>a</sub>** at thermodynamic equilibrium.

Table 4. Differences in Enthalpies and Free Energies of Formation and for Hydrogen Abstraction from DHPs with Iodine atom.<sup>a</sup>

	$\Delta\Delta H_f^\circ$ ( <b>6</b> ) <sup>b</sup>	$\Delta\Delta H_f^\circ$ ( <b>7</b> ) <sup>b</sup>	$\Delta\Delta H_f^\circ$ ( <b>8</b> ) <sup>b</sup>	$\Delta\Delta H_f^\circ$ ( <b>9</b> ) <sup>c</sup>	$\Delta\Delta H_{Rxn}^\circ$ ( <b>6</b> ) <sup>d</sup>	$\Delta\Delta H_{Rxn}^\circ$ ( <b>9</b> ) <sup>d</sup>
<b>(B<sub>a</sub>-C)</b>	-2.6(-1.9)	-1.9(-1.0)	+2.3(+3.2)	+7.8(+8.3)	+1.21(+1.61)	-2.29(-2.89)
<b>(I<sub>a</sub>-L<sub>a</sub>)</b>	-1.2(-0.6)	-0.6(+0.2)	+4.9(+5.5)	+10.1(+11.1)	+2.59(+2.72)	-2.58(-2.64)
<b>(K<sub>a</sub>-J)</b>	-1.0(-0.3)	-0.3(+0.5)	+2.2(+3.5)	+7.0(+7.8)	+0.42(+0.63)	-2.62(-2.59)

a.  $\Delta\Delta G_f^\circ$  in parenthesis. b. In kcal/mol calculated at the B3LYP/6-311+G(2d,p), and, c. at the B3LYP/6-31G(d) computational level. d. Calculated using equation 5.

(3) The relative stabilities of DHP radicals formed in reactions with the iodine atom/radical can also potentially play an important role in the rates of hydrogen abstraction. The relative stability's of radicals generated by abstraction of hydrogen from the terminal unsaturated ring of the DHPs (Series A\* radicals) are given in Table 2. In the reaction of **6** the stability differences between radicals formed from competing DHPs, **B<sub>a</sub>-C**, **I<sub>a</sub>-L<sub>a</sub>**, and **J-K<sub>a</sub>** are very small, -0.4, + 2.1, and -0.4 kcal/mol respectively. In stark contrast, these energy differences, **B<sub>a</sub>-C**, **I<sub>a</sub>-L<sub>a</sub>**, and **J-K<sub>a</sub>**, +5.4, +8.5, and -5.2 kcal/mol respectively, are much larger in the reaction of **9**. These values can be used in conjunction with equation 5 shown in Figure 9 to generate the differences in the enthalpies of reaction for abstraction of the first hydrogen from the competing DHPs with the iodine atom (Table 4 columns 5 and 6). In **6** these endothermic hydrogen abstractions are energetically more favorable from its acene-embedded DHPs, **C**, **L<sub>a</sub>**, and **J**, while in substrate **9** they are more favorable from their helicene-embedded DHPs (Table 4 columns 6 and 7). In both cases, hydrogen abstraction is enthalpically more favorable from the least stable set of DHPs.

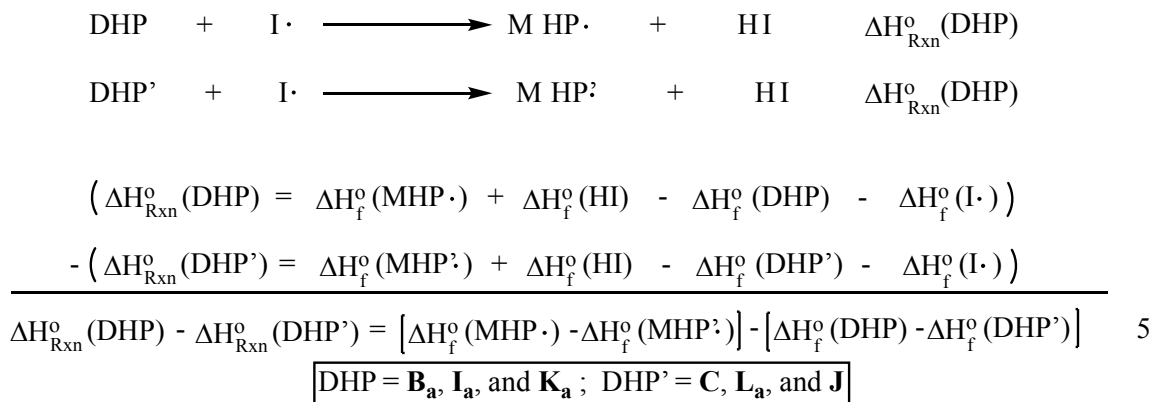


Figure 9. Equation 5 to Determine  $\Delta\Delta H_{\text{Rxn}}^{\circ}$  for **6** and **9** (Table 4).

(4) Increasing temperature can: (a) enhance the rate of passage over the TS<sub>1</sub> barrier on the Mallory photocyclization S<sub>1</sub> PES, (Figure 1) (b) it can increase the rate of thermal decompositions of the DHPs, and (c) it can increase the rate of hydrogen abstraction by iodine atom from the DHPs.

(a) Dulić and coworkers<sup>35</sup> have examined the temperature dependence of passage over the TS<sub>1</sub> barrier for a series of *cis*-stilbene photochromic switches. The rate of approach to the open/closed photostationary state is temperature independent at temperatures above 0°C where most Mallory photocyclizations are conducted. At temperatures below 0°C the quantum yields (e.g.  $\phi_{\text{A} \rightarrow \text{B}}$ ,  $\phi_{\text{J} \rightarrow \text{H}}$ , etc.) may exhibit small changes as a function of temperature, however, to a large extent these changes are likely to cancel each other in the quantum yield ratios (e.g.  $[(\phi_{\text{A} \rightarrow \text{B}})(\phi_{\text{C} \rightarrow \text{A}})]/[(\phi_{\text{B} \rightarrow \text{A}})(\phi_{\text{A} \rightarrow \text{C}})]$ , etc.) that are directly proportional to the steady state concentrations of the competing DHPs (Eqns. 4a, 4b, and 4c). *trans*-Stilbene but not *cis*-stilbene also encounters an activation barrier on the way to the twisted phantom intermediate on its geometric isomerization energy surface and as a result competitive fluorescence is observed in solution for the *trans*- but not the *cis*-isomer.<sup>57</sup> This barrier, however, is only 3.5 kcal/mol<sup>58</sup> and,

1  
2  
3 consequently, unlikely to influence the *cis*-/*trans*-stilbene photostationary state at temperatures  
4 used for Mallory photocyclizations. It is also worthwhile to note that the **13/14** *cis/trans*  
5 photostationary state is established early on the bis-Mallory photocyclization PES (Figure 2) and  
6 is maintained throughout the reaction.  
7  
8  
9  
10

11  
12 (b) DHPs have been directly observed and their thermal decompositions have been  
13 monitored.<sup>54</sup> Lifetimes of the DHPs have also been measured but their accuracy, and what is  
14 really being measured, is debatable because of the wide range of processes including oxidation  
15 and rearrangements that contribute to their decompositions. Nevertheless, the thermal  
16 decompositions of the competing DHP isomers in the blue, red, and green regions of the  
17 interconversion diagram (Scheme 4) with the greatest internal energy are expected to be more  
18 facile. The concerted thermal conrotatory openings of the DHPs reported here are not allowed,  
19 however, their high-energy content ( $> 39$  kcal/mol relative to their styrenyl precursor; Table 1)  
20 provides a driving force for their homolytic cleavage initiated decompositions to regenerate the  
21 Mallory substrates.  
22  
23  
24  
25  
26  
27  
28  
29  
30  
31  
32  
33  
34

35 (c) In DHPs **B<sub>a</sub>**, **I<sub>a</sub>**, and **K<sub>a</sub>** the two hydrogens available for abstraction differ in their  
36 accessibility to the iodine atom and lead to radicals of very different thermodynamic stabilities  
37 (Table 2). In contrast, both hydrogens in DHPs **C**, **J**, and **L<sub>a</sub>** are equally accessible for  
38 abstraction and lead to nearly iso-energetic radicals. Consequently, the rate constants for  
39 hydrogen abstraction will increase with increasing temperature more rapidly for DHPs **C**, **J**, and  
40 **L<sub>a</sub>** than for DHPs **B<sub>a</sub>**, **I<sub>a</sub>**, and **K<sub>a</sub>** since they enjoy an  $R_{ln}2$  symmetry contribution to the entropy  
41 of activation.  
42  
43  
44  
45  
46  
47  
48  
49  
50

51 **Reaction Mechanisms for Mallory Substrates 6, 7, 8, and 9.** The bis-Mallory  
52 photocyclizations of **6**, **7**, **8**, and **9** are very complex reactions, (Scheme 4) and as discussed  
53  
54  
55  
56  
57  
58  
59  
60

1  
2  
3 above, depend upon a myriad of experimental conditions and substrate structural features that  
4 can influence their choice of reaction pathway. Detailed photophysical studies will be required  
5 to unravel the precise mechanistic details for each of these bis-Mallory substrates. Nevertheless,  
6 it is useful to qualitatively examine how the factors discussed above can influence the reaction  
7 pathways and product distributions in these substrates.

8  
9  
10  
11  
12  
13  
14 *Mallory Photocyclization Substrates 6 and 7.* At 0°C and below Mallory substrates **6** and **7**  
15 exclusively produce the helicene products **11a** and **11b**, respectively (Scheme 4). This is  
16 consistent with preferential photostationary formations of **B** and **I**, since the ratio  $\epsilon_C/\epsilon_B$  and  $\epsilon_L/\epsilon_I$   
17 for **6** and **7**, respectively, are equal to the ratios of the oscillator strengths and the smaller  
18 oscillator strength of the DHP precursor to **11a** and **11b** (e.g.  $f_C/f_B(\mathbf{6}) = (0.3135/0.0622) = 5.04$   
19 and  $f_C/f_B(\mathbf{7}) = (0.2946/0.0619) = 4.76$ ; Table 3) means that their concentrations build-up because  
20 they absorb less light. However, in order to attain  $[B]/[C]$  and  $[I]/[L]$  ratios of 20 or greater  
21 (i.e. exclusive detection of **11a** and **11b**), it would also require that  $[(\phi_{A\rightarrow B})(\phi_{C\rightarrow A})]/[(\phi_{B\rightarrow A})(\phi_{A\rightarrow C})]$   
22 and  $[(\phi_{G\rightarrow I})(\phi_{L\rightarrow G})]/[(\phi_{I\rightarrow G})(\phi_{G\rightarrow L})]$  (See Eqn. 4a,b) have values of approximately 4 to 5. We argue  
23 that values of 4 to 5 are reasonable and are consistent with the Laarhoven effect that suggests  
24 (vide supra) that bonding occurs between carbon atoms where the “residual affinity” for bond  
25 formation is the greatest, which in many cases leads to preferential helicene formation.  
26 Consequently, the Laarhoven (kinetic) effect in the photocyclizations of **6** and **7** requires the blue  
27 quantum yields,  $(\phi_{A\rightarrow B})$  and  $(\phi_{G\rightarrow I})$ , involving formation or extension of a helical structure to be  
28 larger than the red quantum yields,  $(\phi_{B\rightarrow A})$  and  $(\phi_{I\rightarrow G})$  that involve loss or decrease of helical  
29 structure. This observation, coupled with the fact that the black quantum yields for the photo-  
30 reversible formation of DHPs, that do not involve formation, extension, loss, or decrease in  
31 helical structure, are more comparable in magnitude,  $(\phi_{C\rightarrow A}) \approx (\phi_{A\rightarrow C})$  and  $(\phi_{L\rightarrow G}) \approx (\phi_{G\rightarrow L})$  support  
32  
33  
34  
35  
36  
37  
38  
39  
40  
41  
42  
43  
44  
45  
46  
47  
48  
49  
50  
51  
52  
53  
54  
55  
56  
57  
58  
59  
60

our contention that values of 4 to 5 for the ratio of quantum yields in equations **4a** and **4b** are reasonable. As the temperature is raised the photostationary state favoring helicene formation is not established, instead, for example, in the case of **6**, the 3.65 kcal/mol and 1.94 kcal/mol (Table 4) energetically preferred hydrogen abstractions from DHPs **C** and **J**, respectively, serve to shift the  $\mathbf{B} \rightleftharpoons \mathbf{C}$  and  $\mathbf{K} \rightleftharpoons \mathbf{J}$  equilibrium towards these more stable DHPs and ultimately produce the high temperature products **12a** and **12b**.

*Mallory Photocyclization Substrate 8.* At 0°C the helicene, **11c**, is the exclusive product of the Mallory photocyclization of **8**. However, the concentration of the dibenzopentaphene product, **12c**, becomes approximately equal to the concentration of **11c** at 30°C to 40°C at lower temperatures than observed for **6** and **7** (Figure 3). This is consistent with the observation that DHPs, **C** and **J**, on the way to **12c** are 3.2 and 3.5 kcal/mol more stable than their competitively formed DHPs **B<sub>a</sub>** and **K<sub>a</sub>**, respectively (Tables 1 and 4). Consequently, the rates of hydrogen abstraction,  $k_C[\mathbf{C}][\mathbf{I}]$  and  $k_J[\mathbf{J}][\mathbf{I}]$ , because of the higher concentrations of **C** and **J**, can more effectively compete with establishment of the photostationary state and enhance the amount of **12c** formed in the photocyclization. In comparison, in the reactions of **6** and **7**, DHPs, **C** and **J**, on the way to **12a** and **12b**, respectively, are far less stable relative to their competitively formed DHPs **B<sub>a</sub>** and **K<sub>a</sub>** (Tables 1 and 4). As a consequence formation of **12a** and **12b** do not compete as effectively with formation of **11a** and **11b** and a higher temperature is required for their concentrations to become equal (i.e.  $[\mathbf{12a}] = [\mathbf{11a}]$  and  $[\mathbf{12b}] = [\mathbf{11b}]$ ).

*Mallory Photocyclization Substrate 9.* Photocyclization of **9** at -30°C unexpectedly generated benzo[k]naphtho[1,2-a]tetrphene, **10d**, as the only product (Figure 3d). In contrast to the other two possible regioisomers, **11d** and **12d**, it can form either in the red or green regions of the interconversion diagram shown in Scheme 4. However, irradiation of **9** is anticipated to

1  
2  
3 predominantly generate DHP **C** because it is 9 kcal/mol more stable than **B<sub>a</sub>** (Table 1).  
4  
5 Nevertheless, at -30°C hydrogen abstraction from DHP **C** does not enjoy as large a symmetry  
6  
7 advantage ( $T\Delta S = T\ln 2$ ) as it would have at higher temperatures, and its lifetime is extended  
8  
9 sufficiently to allow formation of the photostationary state and DHP **B<sub>a</sub>**. Hydrogen abstraction to  
10  
11 form **G** followed by exclusive photocyclization to form **L<sub>a</sub>**, driven by its very large  
12  
13 thermodynamic stability (11.6 kcal/mol) relative to **I<sub>a</sub>**, (Table 1) subsequently generates the  
14  
15 observed product, **10d**. (Note: for comparison **I<sub>a</sub>** and **L<sub>a</sub>** formed in the photocyclizations of **6** and  
16  
17 **7** (Table 1) are nearly identical in energy) This scenario is supported by the fact that at slightly  
18  
19 higher temperatures the less stable **I<sub>a</sub>** is increasingly populated and **11d** forms but then decreases  
20  
21 (Figure 3) as it succumbs to the thermodynamic stability's of DHPs **C**, and **J** on the way to the  
22  
23 thermodynamically most stable regioisomer **12d**.  
24  
25  
26  
27  
28  
29  
30

## 31 CONCLUSIONS

32  
33 Mallory substrates, **6**, **7**, and **8**, react at low temperatures to exclusively produce  
34  
35 their helicene products, **11a**, **11b**, and **11c**, despite the fact that their regioisomers, **10a**,  
36  
37 **10b**, and **10c**, that can form competitively are 11.0, 10.7, and 12.2 kcal/mol more stable.  
38  
39 This unusual, and synthetically useful, observation can be attributed to three effects: (1)  
40  
41 the energies of the DHP precursors to these two sets of regioisomers are much closer in  
42  
43 energy ( $\leq 5.5$  kcal/mol) than the 10.7-12.2 kcal/mol separating the energies of the final  
44  
45 regioisomeric products; (2) the extinction coefficients of the DHP precursors to the  
46  
47 helicenes are smaller than the extinction coefficients of DHP precursors to their  
48  
49 regioisomers by a factor of 4.8 to 9.2; and (3) at low temperatures thermal decompositions  
50  
51 of intermediates are suppressed. Consequently, these effects allow attainment of the  
52  
53  
54  
55  
56  
57  
58  
59  
60

1  
2  
3 photostationary state while suppressing thermal decomposition of the DHPs and  
4  
5 simultaneously bias the photostationary state towards population of the DHP precursor to  
6  
7 the helicene product. This provides a satisfying and compelling rationale for what many  
8  
9 feel is the most bizarre feature of Mallory photocyclization reactions; the preferential  
10  
11 formation of the thermodynamically least stable helicene regioisomer.  
12  
13

14  
15 Unparalleled control over product regiochemistry in Mallory photocyclizations is  
16  
17 now available by rationale design of substrates to influence dihydrophenanthrene (DHP)  
18  
19 intermediate stability and the magnitudes of their extinction coefficients. These structural  
20  
21 controls coupled with the ability to use temperature to influence approach to the DHP  
22  
23 photostationary state enhances the utility of one of the most widely used photochemical  
24  
25 methods for formation of polycyclic aromatic hydrocarbons.  
26  
27  
28  
29  
30

## 31 EXPERIMENTAL

32  
33  
34 *3,6-dibromobenzo[ff]tetraphene*. A  $\text{CH}_2\text{Cl}_2$  (32 mL) suspension of 3,6-  
35  
36 dibromophenanthrenequinone (0.25g, 0.68 mmol) and *o*-xylylenebis(triphenylphosphonium  
37  
38 bromide) (0.625g, 0.79 mmol) was stirred until homogenous. The stir bar was removed and 15  
39  
40 ml of freshly prepared LiOH solution (3.36 M, 0.35 g Li metal in 15 ml water) was added. The  
41  
42 two-phase mixture was sonicated for 80 min. The reaction product was extracted with  $\text{CH}_2\text{Cl}_2$   
43  
44 and washed with water. The crude product was purified by silica gel chromatography (toluene)  
45  
46 and was finally recrystallized from the eluent to give (90 mg, 30%) of 2, 13-  
47  
48 dibromobenzo[*b*]triphenylene as colorless needles.  $^1\text{H}$  NMR (400 MHz,  $\text{CDCl}_3$ ,  $\delta$ ): 7.58-7.60 (m,  
49  
50 2H), 7.76 (dd,  $J = 1.9$  Hz, 8.7 Hz, 2H), 8.05-8.07 (m, 2H), 8.55 (d,  $J = 1.9$  Hz, 2H), 8.58 (d,  $J =$   
51  
52 8.8 Hz, 2H), 8.97 (s, 2H).  $^{13}\text{C}\{^1\text{H}\}$  NMR (100 MHz,  $\text{CDCl}_3$ ,  $\delta$ ): 122.4 (2C), 122.4 (2C), 125.7  
53  
54  
55  
56  
57  
58  
59  
60

(2C), 126.6 (2C), 126.8 (2C), 127.6 (2C), 128.3 (2C), 129.5 (2C), 130.8 (2C), 131.3 (2C), 132.6 (2C). See the Supporting information on the details of the X-ray structure of 2,13-dibromobenzo[b]triphenylene.

*3,6-di((E)-styryl)benzo[ff]tetraphene (8)*. A mixture of 2,13-dibromobenzo[b]triphenylene (66.5 mg, 0.14 mmol), tetra-n-butylammonium bromide (108 mg, 0.34 mmol), and K<sub>2</sub>CO<sub>3</sub> (84.4 mg, 0.61 mmol) in 4 ml DMA was stirred and heated to 120°C under nitrogen. When 60°C was reached, the reaction mixture was charged with styrene (47.5 mg, 0.46 mmol). When 90°C was reached a prepared palladium catalyst solution was added drop-wise (Pd(OAc)<sub>2</sub> (0.7 mg, 3 μmol), 1,3-bis(diphenylphosphino)propane (1.9 mg, 4.6 μmol) in 4 ml DMA). This reaction was then stirred at 120°C for 48 h and then allowed to cool to room temperature and transferred to a separatory funnel along with 25 ml of 6 N HCl. The reaction product was extracted with CH<sub>2</sub>Cl<sub>2</sub> and washed with 6N HCl and water. Removal of the solvent produced an off-white solid in nearly quantitative yield that was used in the next step without purification. An analytically pure sample for characterization was obtained by washing with acetone to give a white solid. (30 mg, 44%) <sup>1</sup>H NMR (400 MHz, CDCl<sub>3</sub>, δ): 7.32-7.48 (m, 10H), 7.58-7.61 (m, 2H), 7.68 (d, J = 8.1 Hz, 4H), 7.93 (dd, J = 1.4 Hz, 8.5 Hz, 2H), 8.11-8.13 (m, 2H), 8.71 (d, J = 1.5 Hz, 2H), 8.79 (d, J = 8.6 Hz, 2H), 9.09 (s, 2H). <sup>13</sup>C{<sup>1</sup>H} NMR (100 MHz, CDCl<sub>3</sub>, δ): 122.2 (2C), 122.2 (2C), 122.3 (2C), 124.3 (2C), 125.2 (2C), 126.2 (2C), 126.7 (4C), 127.9 (2C), 128.2 (2C), 128.4 (2C), 128.8 (4C), 128.8 (2C), 128.9 (2C), 129.6 (2C), 129.9 (2C), 132.4 (2C), 136.7 (2C). HRMS (MALDI-TOF) *m/z* calculated for C<sub>38</sub>H<sub>27</sub> [M+H]<sup>+</sup>, 483.2113, found 483.2144.

*3,6-di((E)-styryl)-9,10-bis-ethyleneketalphenanthrene (9)*. A mixture of 3,6-dibromo-9,10-bis-ethyleneketalphenanthrene (280 mg, 0.62 mmol), tetra-n-butylammonium bromide (480 mg, 1.49 mmol), and K<sub>2</sub>CO<sub>3</sub> (103 mg, 0.74 mmol) in 6 ml DMA was stirred and heated up to 120°C under

1  
2  
3 nitrogen. When 60°C was reached, the reaction mixture was charged with styrene (193 mg, 1.86  
4 mmol). When 90°C was reached a prepared palladium catalyst solution was added drop-wise  
5  
6 (Pd(OAc)<sub>2</sub> (28 mg, 0.12 mmol), 1,3-bis(diphenylphosphino)propane (77 mg, 0.19 mmol) in 6 ml  
7 DMA). This reaction mixture was then allowed to stir at 120°C for 48 h followed by removal of  
8 the DMA using a vacuum oven. The residue was then treated with hot ethanol and filtered.  
9  
10 Recrystallization in EtOH gave **9** (120 mg, 39%) as off-white crystals. <sup>1</sup>H NMR (400 MHz,  
11 CDCl<sub>3</sub>, δ): 3.69 (broad s, 4H), 4.22 (broad s, 4H), 7.27-7.41 (m, 8H), 7.57-7.62 (m, 8H), 7.76 (d,  
12 J = 8.0 Hz, 2H), 8.06 (s, 2H). <sup>13</sup>C{<sup>1</sup>H} NMR (100 MHz, CDCl<sub>3</sub>, δ): 61.7 (broad, 4C), 92.9 (2C),  
13 122.5 (2C), 126.7 (2C), 126.9 (2C), 126.9 (4C), 128.1 (2C), 128.4 (2C), 129.0 (4C), 130.1 (2C),  
14 132.5 (4C), 133.5 (2C), 137.3 (2C), 139.2 (2C). HRMS(MALDI-TOF) m/z calculated for  
15 C<sub>34</sub>H<sub>28</sub>O<sub>4</sub> [M]<sup>+</sup> 500.1988, found 500.1984.  
16  
17  
18  
19  
20  
21  
22  
23  
24  
25  
26  
27

28 *General procedure for Mallory bis-photocyclization-dehydrogenation.* A solution of the  
29 bisstyrylphenanthrene substrate (0.5 mM), I<sub>2</sub> (2.2 molar equivalent), and propylene oxide (50  
30 molar equivalent) in toluene was heated or cooled to the desired temperature and subsequently  
31 irradiated overnight in a Pyrex vessel with a 600W medium pressure mercury vapor lamp. The  
32 reaction mixture was allowed to cool or warm to room temperature and was washed with sodium  
33 thiosulfate 3X's and DI water 3X's and finally with brine. The toluene was removed and the  
34 sample was dried in a vacuum oven overnight prior to NMR analysis. No precipitate was visible  
35 in any of the NMR samples.  
36  
37  
38  
39  
40  
41  
42  
43  
44  
45

46 *5,6-Bis-ethyleneketal-naphtho[2,1-b]pentahelicene (10d).* A solution of **9** (100 ml, 0.5 mM), I<sub>2</sub>  
47 (1.1 mM), and propylene oxide (25 mM) in toluene was placed in an ice-bath. The reaction  
48 mixture temperature was maintained at 0°C and irradiated for 13 hours with a 600W medium  
49 pressure mercury vapor lamp. The organic reaction product was washed with sodium thiosulfate  
50  
51  
52  
53  
54  
55  
56  
57  
58  
59  
60

1  
2  
3 3X's and water 3X's and dried over MgSO<sub>4</sub>. The solvent was removed at reduced pressure and  
4 the crude product was purified by silica gel chromatography (1:4 EtOAc : hexanes) to give **10d**  
5 as a colorless solid. <sup>1</sup>H NMR (600 MHz, CDCl<sub>3</sub>, δ): 3.40 (d, J = 11.1 Hz, 1H), 3.53 (dd, J = 2.3  
6 Hz, 11.1 Hz, 1H), 3.79 (td, J = 2.5 Hz, 12.3 Hz, 1H), 3.94 (dd, J = 2.1 Hz, 12.0 Hz, 1H), 4.11 (d,  
7 J = 7.3 Hz, 2H), 4.60-4.68 (m, 2H), 7.0 (t, J = 7.7 Hz, 1H), 7.34 (d, J = 8.9 Hz, 1H), 7.42 (t, J =  
8 7.0 Hz, 1H), 7.61 (t, J = 7.2 Hz, 1H), 7.63 (d, 8.7 Hz, 1H), 7.69 (t, J = 7.7, 1H), 7.73 (d, J = 8.7  
9 Hz, 1H), 7.80 (d, J = 8.8 Hz, 1H), 7.85 (d, J = 8.4 Hz, 1H), 7.87 (s, 2H), 8.14 (s, 1H), 8.36 (d, J =  
10 8.6 Hz, 1H), 8.81 (d, J = 8.3 Hz, 1H), 9.09 (s, 1H). <sup>13</sup>C{<sup>1</sup>H} NMR (100 MHz, CDCl<sub>3</sub>, δ): 59.1  
11 (1C), 59.4 (1C), 63.5 (1C), 63.9 (1C), 92.7 (1C), 93.2 (1C), 120.4 (1C), 123.0 (1C), 123.6 (1C),  
12 124.1 (1C), 126.5 (1C), 126.7 (1C), 126.8 (1C), 126.9 (1C), 126.9 (1C), 127.7 (1C), 127.8 (1C),  
13 128.0 (1C), 128.0 (1C), 128.6 (1C), 129.5 (1C), 129.5 (1C), 129.6 (1C), 129.6 (1C), 130.3 (1C),  
14 130.4 (1C), 130.8 (1C), 131.9 (1C), 132.3 (1C), 132.4 (1C), 132.7 (1C), 133.1 (1C), 133.3 (1C),  
15 134.8 (1C). HRMS (MALDI-TOF) *m/z* calculated for C<sub>34</sub>H<sub>24</sub>O<sub>4</sub> [M]<sup>+</sup>, 496.1675, found 496.1680.  
16  
17  
18  
19  
20  
21  
22  
23  
24  
25  
26  
27  
28  
29  
30  
31  
32  
33 *Naphtho[2,3-*l*]heptahelicene (11c)*. To a solution of 9,10-[7]helicenequinone (6.2 mg, 15.2  
34 μmol), O-xylenebis(triphenylphosphonium bromide) (21.5 mg, 27.4 μmol), and tetra-*n*-  
35 butylammonium perchlorate (3 mg, 8.8 μmol) in CH<sub>2</sub>Cl<sub>2</sub> (2ml) 2 ml of freshly prepared LiOH  
36 solution (0.5 M, 7 mg Li metal in 2 ml water) was added. The two-phase mixture was sonicated  
37 for 90 min. The reaction product was extracted with toluene and washed with water. The crude  
38 product was purified by silica gel chromatography (100% hexanes) to give **11c** (1.3 mg, 18%) as  
39 a pale yellow solid. <sup>1</sup>H NMR (600 MHz, CDCl<sub>3</sub>, δ): 6.43 (ddd, J = 1.3 Hz, 6.8 Hz, 8.3 Hz, 2H),  
40 6.89 (d, J = 8.5, 2H), 6.93 (ddd, J = 1.1 Hz, 6.8 Hz, 7.87 Hz, 2H), 7.27 (d, J = 7.9 Hz, 2H), 7.40  
41 (d, J = 8.5 Hz, 2H), 7.62-7.63 (m, 2H), 7.67 (d, J = 8.5 Hz, 2H), 8.07 (d, J = 8.4 Hz, 2H), 8.19-  
42 8.21 (m, 2H), 8.95 (d, J = 8.6 Hz, 2H), 9.27 (s, 2H). <sup>13</sup>C{<sup>1</sup>H} NMR (100 MHz, CDCl<sub>3</sub>, δ): 121.2  
43  
44  
45  
46  
47  
48  
49  
50  
51  
52  
53  
54  
55  
56  
57  
58  
59  
60

1  
2  
3 (2C), 122.3 (2C), 123.6 (2C), 125.0 (2C), 125.4 (2C), 125.4 (2C), 126.0 (2C), 126.1 (2C), 126.5  
4 (2C), 127.2 (2C), 127.9 (2C), 128.3 (2C), 129.0 (2C), 129.6 (2C), 129.7 (2C), 129.8 (2C), 131.7  
5 (2C), 131.8 (2C), 132.4 (2C). HRMS (MALDI-TOF)  $m/z$  calculated for  $C_{38}H_{22} [M]^+$ , 478.1722,  
6 found 478.1717.  
7  
8  
9

10  
11  
12 *Dibenzo[c,m]-naphtho[2,3,h]pentaphene (12c)*. A solution of crude **8** (100 mg, 0.21 mmol),  
13  $I_2$  (116 mg, 0.46 mmol), and propylene oxide (725  $\mu$ L, 103.6 mmol) in toluene (420 ml) was  
14 heated up to 95°C in a 500 ml Pyrex flask. Once the target temperature was reached, the sample  
15 was irradiated with a 600 W medium pressure mercury vapor lamp for 20 hours. The reaction  
16 solution was allowed to cool to room temperature and then washed with sodium thiosulfate to  
17 remove unreacted iodine and subsequently washed with water. The reaction product was passed  
18 through a silica gel plug using toluene to give **12c** (57.2 mg, 58%) as a yellow solid.  $^1H$  NMR  
19 (400 MHz,  $CDCl_3$ ,  $\delta$ ): 7.61 (dd,  $J = 7.8$  Hz, 7.8 Hz, 2H), 7.69 (dd,  $J = 7.7$  Hz, 7.7 Hz, 2H), 7.72-  
20 7.73 (m, 2H), 7.87 (d,  $J = 7.6$  Hz, 2H), 8.36-8.37 (m, 2H), 8.59-8.66 (m, 4H), 8.77 (d,  $J = 8.5$  Hz,  
21 2H), 8.82 (d,  $J = 8.82$  Hz, 2H), 9.67 (dd,  $J = 3$  Hz, 8.7 Hz, 2H), 9.78 (d,  $J = 5.6$  Hz, 2H). HRMS  
22 (MALDI-TOF)  $m/z$  calculated for  $C_{38}H_{22} [M]^+$ , 478.1722, found 478.1714.  
23  
24  
25  
26  
27  
28  
29  
30  
31  
32  
33  
34  
35  
36

37  
38 *7,8-bis-ethyleneketal-dibenzo[c,m]pentaphene (12d)*. A solution of **9** (100 ml, 0.5 mM),  $I_2$  (1.1  
39 mM), and propylene oxide (25 mM) in toluene was prepared in a 250 ml Pyrex glass pressure  
40 vessel. The reaction mixture was heated to 157°C and subsequently irradiated for 18 hours with a  
41 600W medium pressure mercury vapor lamp. The reaction mixture was washed with sodium  
42 thiosulfate 3X's and water 3X's and dried over  $MgSO_4$ . The solvent was removed at reduced  
43 pressure and the reaction product was purified by recrystallization in toluene/EtOH to afford **12d**  
44 as a colorless solid.  $^1H$  NMR (600 MHz,  $CDCl_3$ ,  $\delta$ ): 3.84 (Broad s, 4H), 4.41 (Broad s, 4H), 7.64  
45 (ddd,  $J = 1.0$  Hz, 7.1 Hz, 7.9 Hz, 2H), 7.70 (ddd,  $J = 1.3$  Hz, 7.1 Hz, 8.2 Hz, 2H), 7.82 (d,  $J = 8.8$   
46  
47  
48  
49  
50  
51  
52  
53  
54  
55  
56  
57  
58  
59  
60

1  
2  
3 Hz, 2H), 7.89 (d, J = 8.8 Hz, 2H), 7.92 (d, 7.8 Hz, 2H), 8.62 (s, 2H), 8.82 (d, 8.3 Hz, 2H), 9.14 (s,  
4 2H).  $^{13}\text{C}\{^1\text{H}\}$  NMR (100 MHz,  $\text{CDCl}_3$ ,  $\delta$ ): 93.3 (2C), 121.1 (2C), 123.1 (2C), 124.2 (2C), 126.8  
5 (2C), 126.9 (2C), 127.0 (2C), 128.3 (2C), 128.7 (2C), 130.4 (2C), 130.6 (2C), 131.3 (2C), 131.3  
6 (2C), 132.2 (2C), 133.2 (2C). HRMS (MALDI-TOF)  $m/z$  calculated for  $\text{C}_{34}\text{H}_{24}\text{O}_4$   $[\text{M}]^+$ ,  
7 496.1675, found 496.1676.  
8  
9

10  
11  
12  
13  
14 *3,6-Bis-styrylphenanthrenequinone*. A mixture of 3,6-dibromophenanthrenequinone (100 mg,  
15 0.27 mmol), tetra-*n*-butylammonium bromide (35 mg, 0.11 mmol), and  $\text{K}_2\text{CO}_3$  (189 mg, 1.37  
16 mmol) in 1.5 ml DMA was stirred and heated up to 120°C under nitrogen for 48 hours. When  
17 60°C was reached, the reaction mixture was charged with styrene (85 mg, 0.82 mmol). When  
18 90°C was reached a prepared palladium catalyst solution was added drop-wise ( $\text{Pd}(\text{OAc})_2$  (0.6  
19 mg, 2.7  $\mu\text{mol}$ ), 1,3-Bis(diphenylphosphino)propane (1.4 mg, 3.28  $\mu\text{mol}$ ) in 1.5 ml DMA). The  
20 DMA was removed using a vacuum oven. The reaction product was purified by silica gel  
21 chromatography (3:2 Hexanes: Ethyl acetate) to afford 3,6-bis-styrylphenanthrenequinone (20.8  
22 mg, 19%) as a red film.  $^1\text{H}$  NMR (400 MHz,  $\text{CDCl}_3$ ,  $\delta$ ): 7.26 (d, J = 7.8 Hz, 16.0 Hz, 2H), 7.34-  
23 7.45 (m, 8H), 7.62 (d, J = 7.7 Hz, 4H), 7.67 (d, 8 Hz, 2H), 8.15 (s, 2H), 8.23 (d, J = 8.1 Hz, 2H).  
24  
25

26  
27  
28  
29  
30  
31  
32  
33  
34  
35  
36  
37 *5,6-Dimethoxy-2-pentahelicenecarboxaldehyde (15b)*. A solution of **7** (100 ml, 0.5 mM),  $\text{I}_2$  (2.2  
38 molar equivalent), and propylene oxide (50 molar equivalent) in toluene was irradiated overnight  
39 with a 600W medium pressure mercury vapor lamp. The organic reaction product was washed  
40 with sodium thiosulfate 3X's and water 3X's and dried over  $\text{MgSO}_4$ . The toluene was filtered  
41 and removed under reduced pressure and the crude reaction product was purified by silica gel  
42 chromatography (1% EtOAc in hexanes) to afford **15b** as a yellow solid.  $^1\text{H}$  NMR (600 MHz,  
43  $\text{CDCl}_3$ ,  $\delta$ ): 4.20 (s, 3H), 4.21 (s, 3H), 7.24 (ddd, J = 1.4 Hz, 7.0 Hz, 8.3 Hz, 1H), 7.53 (ddd, J =  
44 1.0 Hz, 7.0 Hz, 7.9 Hz, 1H), 7.91 (d, J = 8.5 Hz, 1H), 7.96-7.99 (m, 3H), 8.02 (dd, J = 1.5 Hz,  
45  
46  
47  
48  
49  
50  
51  
52  
53  
54  
55  
56  
57  
58  
59  
60

1  
2  
3 8.6 Hz, 1H), 8.31 (d, 8.5 Hz, 1H), 8.39 (d, 8.4 Hz, 1H), 8.40 (d, 8.5 Hz, 1H), 8.92 (s, 1H), 9.72 (s,  
4 1H).  $^{13}\text{C}\{^1\text{H}\}$  NMR (100 MHz,  $\text{CDCl}_3$ ,  $\delta$ ): 61.5 (1C), 61.5 (1C), 121.1 (1C), 122.9 (1C), 123.5  
5 (1C), 124.9 (1C), 125.8 (1C), 126.5 (1C), 126.9 (1C), 127.0 (1C), 128.1 (1C), 128.3 (1C), 128.4  
6 (1C), 128.6 (1C), 128.7 (1C), 130.0 (1C), 130.7 (1C), 132.0 (1C), 132.3 (1C), 132.7 (1C), 133.1  
7 (1C), 135.9 (1C), 144.4 (1C), 146.9 (1C), 192.6 (1C). HRMS (MALDI-TOF)  $m/z$  calculated for  
8  $\text{C}_{25}\text{H}_{18}\text{O}_3$   $[\text{M}]^+$ , 366.1256, found 366.1257.  
9  
10  
11  
12  
13  
14  
15  
16

17 *Naphtho[2,3-*ff*]-2-pentahelicenecarboxylaldehyde (15c)*. A solution of **8** (100 ml, 0.5 mM),  $\text{I}_2$   
18 (2.2 molar equivalent), and propylene oxide (50 molar equivalent) in toluene was placed in an  
19 ice-bath and irradiated for 14 hours with a 600W medium pressure mercury vapor lamp. The  
20 organic reaction product was washed with sodium thiosulfate 3X's and water 3X's and dried  
21 over  $\text{MgSO}_4$ . The toluene was filtered and removed under reduced pressure and the reaction  
22 product was purified by silica gel chromatography (1% EtOAc in hexanes) to afford (**15c**) as a  
23 yellow solid.  $^1\text{H}$  NMR (600 MHz,  $\text{CDCl}_3$ ,  $\delta$ ): 7.21 (ddd,  $J = 1.3$  Hz, 6.8 Hz, 8.3 Hz, 1H), 7.51  
24 (ddd,  $J = 1.0$  Hz, 6.8 Hz, 7.9 Hz, 1H), 7.63-7.65 (m, 2H), 7.89 (d, 8.5 Hz, 1H), 7.92 (d, 8.6 Hz,  
25 1H), 7.95 (dd,  $J = 1.0$  Hz, 8.0 Hz, 1H), 8.05 (d, 8.3 Hz, 1H), 8.06 (dd,  $J = 1.6$  Hz, 8.3 Hz, 1H),  
26 8.14-8.19 (m, 2H), 8.38 (d, 8.4 Hz, 1H), 8.73 (d, 1.2 Hz, 1H), 8.74 (d, 8.6 Hz, 1H), 8.80 (d, 8.3  
27 Hz, 1H), 9.07 (s, 1H), 9.19 (s, 1H), 9.73 (s, 1H).  $^{13}\text{C}\{^1\text{H}\}$  NMR (100 MHz,  $\text{CDCl}_3$ ,  $\delta$ ): 121.5  
28 (1C), 123.1 (1C), 123.4 (1C), 124.8 (1C), 124.9 (1C), 125.2 (1C), 126.2 (1C), 126.6 (1C), 126.8  
29 (1C), 126.9 (1C), 126.9 (1C), 127.5 (1C), 128.0 (1C), 128.2 (1C), 128.3 (1C), 128.4 (1C), 128.4  
30 (1C), 128.7 (1C), 129.0 (1C), 129.3 (1C), 130.5 (1C), 131.2 (1C), 131.4 (1C), 132.2 (1C), 132.9  
31 (1C), 133.1 (1C), 133.2 (1C), 133.4 (1C), 134.9 (1C), 135.6 (1C), 192.1 (1C). HRMS (MALDI-  
32 TOF)  $m/z$  calculated for  $\text{C}_{31}\text{H}_{18}\text{O}$   $[\text{M}]^+$ , 406.1358, found 406.1358.  
33  
34  
35  
36  
37  
38  
39  
40  
41  
42  
43  
44  
45  
46  
47  
48  
49  
50  
51  
52  
53  
54  
55  
56  
57  
58  
59  
60

1  
2  
3  
4  
5  
6 ASSOCIATED CONTENT  
7

8 **Supporting Information**  
9

10 The supporting Information is available free of charge on the ACS Publications website at DOI:

11  
12  
13 XXXXXXXX  
14

15 Proton and carbon NMR data, X-ray data, cif report, computational details.  
16

17  
18 AUTHOR INFORMATION  
19

20 **Corresponding Author**  
21

22 \*clennane@uwyo.edu  
23

24 ORCID  
25

26  
27 Edward L. Clennan: 0000-0002-9851-1129  
28

29 Jacob Weber: 0000-0002-7756-6382  
30  
31  
32  
33

34 **Notes**  
35

36 The authors declare no competing financial interest.  
37

38  
39 ACKNOWLEDGMENTS  
40

41 This material is based upon work supported by the National Science Foundation under CHE-  
42 1147542 and CHE-1762161. In memory of Frank Mallory 1933-2017.  
43  
44  
45  
46  
47

48  
49 REFERENCES  
50

- 51 1. Smakula, A. The photochemical transformation of *trans*-stilbene. *Z. Physik. Chem.* **1934**,  
52 *B25*, 90-98.  
53 2. Parker, C. O.; Spierri, P. E. Photochemical Conversion of Stilbene to Phenanthrene.  
54 *Nature* **1950**, *166*, 603.  
55  
56  
57  
58  
59  
60

3. Mallory, F. B.; Wood, C. S.; Gordon, J. T.; Lindquist, L. C.; Savitz, M. L. Photochemistry of Stilbenes. I. *J. Am. Chem. Soc.* **1962**, *84*, 4361-4362.
4. Moore, W. M.; Morgan, D. D.; Stermitz, F. R. The Photochemical Conversion of Stilbene to Phenanthrene. The Nature of the Intermediate. *J. Am. Chem. Soc.* **1963**, *85*, 829-830.
5. Doyle, T. D.; Filipescu, N.; Benson, W. R.; Banes, D. Photocyclization of a, a' -Diethyl-4,4'-stilbenediol. Isolation of a Stable Tautomer of the Elusive Dihydrophenanthrenes. *J. Am. Chem. Soc.* **1970**, *92*, 6371-6372.
6. Doyle, T. D.; Benson, W. R.; Filipescu, N. Photocyclization of Diethylstilbestrol. Isolation of a Stable, Self-Trapping Dihydrophenanthrene Intermediate. *J. Am. Chem. Soc.* **1976**, *98*, 3262-3267.
7. Cuppen, J. H. M.; Laarhoven, W. H. Photodehydrocyclizations of Stilbene-Like Compounds. VI. Chemical Evidence of an Excited State Mechanism. *J. Am. Chem. Soc.* **1972**, *94*, 5914-5915.
8. Irie, M.; Fukaminato, T.; Matsuda, K.; Kobatake, S. Photochromism of Diarylethene Molecules and Crystals: Memories, Switches, and Actuators. *Chem. Rev.* **2014**, *114*, 12174-12277.
9. Flammang-Barbieux, M.; Nasielski, J.; Martin, R. H. Synthesis of heptahelicene (1) benzo [c] phenanthro [4, 3-g ]phenanthrene. *Tetrahedron Lett.* **1967**, *8*, 743-744.
10. Martin, R. H. The Helicenes. *Angew. Chem. Int. Ed. Engl.* **1974**, *13*, 649-660.
11. Gingras, M. One hundred years of helicene chemistry. Part 3: applications and properties of carbohelicenes. *Chem. Soc. Rev.* **2013**, *42*, 1051-1095.
12. Gingras, M. One hundred years of helicene chemistry. Part 1: non-stereoselective syntheses of carbohelicenes. *Chem. Soc. Rev.* **2013**, *42*, 968-1006.
13. Gingras, M.; Felix, G.; Peresutti, R. One hundred years of helicene chemistry. Part 2: stereoselective synthesis and chiral separations of carbohelicenes. *Chem. Soc. Rev.* **2013**, *42*, 1007-1050.
14. Laarhoven, W. H. Photochemical cyclizations and intramolecular cycloadditions of conjugated aryl olefins. Part I. Photocyclization with dehydrogenation. *Rec. Trav. Chim.-J. Roy. Neth. Chem.* **1983**, *102*, 185-204.
15. Mallory, F. B.; Mallory, C. W.: Photocyclization of Stilbenes and Related Molecules. In *Organic Reactions*; Dauben, W. G., Ed.; John Wiley & Sons: New York, N.Y., 1984; Vol. 30; pp 1-456.
16. Laarhoven, W. H. Photocyclizations and Intramolecular Photocycloadditions of Conjugated Arylolefins and Related Compounds. *Org. Photochem.* **1989**, *10*, 163-308.
17. Meier, H. The Photochemistry of Stilbenoid Compounds and Their Role in Materials Technology. *Angew. Chem. Int. Ed.* **1992**, *31*, 1399-1420.
18. Tominaga, Y.; Castle, R. N. Photocyclization of aryl- and heteroaryl-2-propenoic acid derivatives. Synthesis of polycyclic heterocycles. *J. Heterocycl. Chem.* **1996**, *33*, 523-538.
19. Hagen, S.; Hopf, H.: Modern routes to extended aromatic compounds. In *Topics in Current Chemistry*; de Meijere, A., Ed.; Carbon Rich Compounds I; Springer-Verlag: Berlin Heidelberg, 1998; Vol. 196; pp 45-89.
20. Liu, L.; Yang, B.; Katz, T. J.; Poindexter, M. K. Improved methodology for photocyclization reactions. *J. Org. Chem.* **1991**, *56*, 3769-3775.
21. Sudhakar, A.; Katz, T. J.; Yang, B. W. Synthesis of a helical metallocene oligomer. *J. Am. Chem. Soc.* **1986**, *108*, 2790-2791.

22. Sudhakar, A.; Katz, T. J. Directive effect of bromine on stilbene photocyclizations. an improved synthesis of [7]helicene. *Tetrahedron Lett.* **1986**, *27*, 2231-2234.
23. Liu, L.; Katz, T. J. Bromine auxiliaries in photosyntheses of [5]helicenes. *Tetrahedron Lett.* **1991**, *32*, 6831-6834.
24. Finnie, A. A.; Hill, R. A. The synthesis of 1,5,7,10-tetraoxygenated 3-methylphenanthrenes. *J. Chem. Res. Synop.* **1987**, 78-79.
25. Mallory, F. B.; Rudolph, M. J.; Oh, S. M. Photochemistry of stilbenes. 8. Eliminative photocyclization of o-methoxystilbenes. *J. Org. Chem.* **1989**, *54*, 4619-4626.
26. Li, Z.; Twieg, R. J. Photocyclodehydrofluorination. *Chem. – European J.* **2015**, *21*, 15534-15539.
27. Morin, J.-F.: Photochemical and Direct C-H Arylation Routes toward Carbon Nanomaterials. In *Synthetic Methods for Conjugated Polymers and Carbon Materials*; 1st ed.; Leclerc, M., Morin, J.-F., Eds.; Wiley-VCH Verlag GmbH & Co. KGaA, 2017; pp 229-253.
28. Ern, J.; Bens, A. T.; Martin, H. D.; Mukamel, S.; Schmid, D.; Tretiak, S.; Tsiper, E.; Kryschi, C. Reaction dynamics of photochromic dithienylethene derivatives. *Chem. Phys.* **1999**, *246*, 115-125.
29. Bens, A. T.; Ern, J.; Kuldova, K.; Trommsdorff, H. P.; Kryschi, C. Reaction and excited state relaxation dynamics of photochromic dithienylethene derivatives. *J. Luminescence* **2001**, *94-95*, 51-54.
30. Hania, P. R.; Telesca, R.; Lucas, L. N.; Pugzlys, A.; van Esch, J.; Feringa, B. L.; Snijders, J. G.; Duppen, K. An Optical and Theoretical Investigation of the Ultrafast Dynamics of a Bisthienylethene-Based Photochromic Switch. *J. Phys. Chem. A* **2002**, *106*, 8498-8507.
31. Bearpark, M. J.; Bernardi, F.; Clifford, S.; Olivucci, M.; Robb, M. A.; Vreven, T. Cooperating Rings in cis-Stilbene Lead to an S0/S1 Conical Intersection. *J. Phys. Chem. A* **1997**, *101*, 3841-3847.
32. Dou, Y.; Allen, R. E. Dynamics of the photocyclization of cis-stilbene to dihydrophenanthrene. *J. Mod. Optics* **2004**, *51*, 2485-2491.
33. Harabuchi, Y.; Keipert, K.; Zahariev, F.; Taketsugu, T.; Gordon, M. S. Dynamics Simulations with Spin-Flip Time-Dependent Density Functional Theory: Photoisomerization and Photocyclization Mechanisms of cis-Stilbene in  $\pi\pi^*$  States. *The J. Phys. Chem. A* **2014**, *118*, 11987-11998.
34. Ioffe, I. N.; Granovsky, A. A. Photoisomerization of Stilbene: The Detailed XMCQDPT2 Treatment. *J. Chem. Theory Computation* **2013**, *9*, 4973-4990.
35. Dulić, D.; Kudernac, T.; Pužys, A.; Feringa, B. L.; van Wees, B. J. Temperature Gating of the Ring-Opening Process in Diarylethene Molecular Switches. *Adv. Mater.* **2007**, *19*, 2898-2902.
36. Sumi, T.; Takagi, Y.; Yagi, A.; Morimoto, M.; Irie, M. Photoirradiation wavelength dependence of cycloreversion quantum yields of diarylethenes. *Chem. Commun.* **2014**, *50*, 3928-3930.
37. Martin, R. H.; Flammang-Barbieux, M.; Cosyn, J. P.; Gelbcke, M. 1-Synthesis of octa- and nonahelicenes. 2-New syntheses of hexa- and heptahelicenes. 3-Optical rotation and O.R.D. of heptahelicene. *Tetrahedron Lett.* **1968**, *9*, 3507-3510.
38. Laarhoven, W. H.; Cuppen, T. H. J. H. M.; Nivard, R. J. F. Photodehydrocyclizations in stilbene-like compounds—III: Effect of steric factors. *Tetrahedron* **1970**, *26*, 4865-4881.

39. Laarhoven, W. H.; Cuppen, T. J. H. M.; Nivard, R. J. F. Photodehydrocyclizations in stilbene-like compounds. *Rec. Trav. Chim.* **1968**, *87*, 687-698.
40. Burkitt, F. H.; Coulson, C. A.; Longuet-Higgins, H. C. Free valence in unsaturated hydrocarbons. *Trans. Faraday Soc.* **1951**, *47*, 553-564.
41. Yuan, Z.; Xiao, Y.; Qian, X. A design concept of planar conjugated ladder oligomers of perylene bisimides and efficient synthetic strategy via regioselective photocyclization. *Chem. Commun.* **2010**, *46*, 2772-2774.
42. Shi, S.; Nawaz, K. S.; Zaman, M. K.; Sun, Z. Advances in Enantioselective C-H Activation/Mizoroki-Heck Reaction and Suzuki Reaction. *Catalysts* **2018**, *8*, 90.
43. Talele, H. R.; Chaudhary, A. R.; Patel, P. R.; Bedekar, A. V. Expedient synthesis of helicenes using an improved protocol of photocyclodehydration of stilbenes. *ARKIVOC* **2011**, *ix*, 15-37.
44. Ben Hassine, B.; Gorsane, M.; Pecher, J.; Martin, R. H. Diastereoselective NaBH<sub>4</sub> Reductions of (dl)  $\alpha$ -Keto Esters. *Bull. Soc. Chim. Belg.* **1985**, *94*, 597-603.
45. Grandbois, A.; Collins, S. K. Enantioselective Synthesis of [7]Helicene: Dramatic Effects of Olefin Additives and Aromatic Solvents in Asymmetric Olefin Metathesis. *Chem. – Euro. J.* **2008**, *14*, 9323-9329.
46. Sapir, M.; Vander Donckt, E. Intersystem Crossing in the Helicenes. *Chem. Phys. Lett.* **1975**, *36*, 108-110.
47. Birks, J. B.; Birch, D. J. S.; Cordemans, E.; Vander Donckt, E. Fluorescence of the higher helicenes. *Chem. Phys. Lett.* **1976**, *43*, 33-36.
48. Grellmann, K.-H.; Hentschel, P.; Wismontski-Knittel, T.; Fischer, E. The photophysics and photochemistry of pentahelicene. *J. Photochem.* **1979**, *11*, 197-213.
49. Wilkinson, F.; Helman, W. P.; Ross, A. B. *J. Phys. Chem. Ref. Data* **1993**, *22*, 113-262.
50. Gorman, A. A.; Gould, I. R.; Hamblett, I. Time-Resolved Study of the Solvent and Temperature Dependence of Singlet Oxygen (<sup>1</sup> $\Delta$ <sub>g</sub>) Reactivity toward Enol Ethers: Reactivity Parameters Typical of Rapid Reversible Exciplex Formation. *J. Am. Chem. Soc.* **1982**, *104*, 7098-7104.
51. Clar, E.: *The Aromatic Sextet*; John Wiley & Sons: London, 1972.
52. Hemelsoet, K.; De Vleeschouwer, F.; Van Speybroeck, V.; De Proft, F.; Geerlings, P.; Waroquier, M. Validation of DFT-Based Methods for Predicting Qualitative Thermochemistry of Large Polyaromatics. *ChemPhysChem* **2011**, *12*, 1100-1108.
53. Wismontski-Knittel, T.; Kaganowitch, M.; Seger, G.; Fischer, E. The reversible photochemistry of 1,2-di-(2-naphthyl)cyclopentene. *Rec. Trav. Chim.* **1979**, *98*, 114-117.
54. Muszkat, K. A. The 4a, 4b-Dihydrophenanthrenes. *Topics Curr. Chem.* **1980**, *38*, 89-143.
55. Hammond, G. S.; Saltiel, J.; Lamola, A. A.; Turro, N. J.; Bradshaw, J. S.; Cowan, D. O.; Counsell, R. C.; Vogt, V.; Dalton, C. Mechanisms of Photochemical Reactions in Solution. XXII.1 Photochemical cis-trans Isomerization. *J. Am. Chem. Soc.* **1964**, *86*, 3197-3217.
56. Klan, P.; Wirz, J.: *Photochemistry of Organic Compounds. From Concepts to Practice*; John Wiley & Sons Ltd.: UK, 2009.
57. Saltiel, J.; Charlton, J. L.: *Rearrangements in Ground and Excited States*; Academic Press: New York, 1980; Vol. 42/43.
58. Fleming, G. R. Subpicosecond Spectroscopy. *Ann. Rev. Phys. Chem.* **1986**, *37*, 81-104.

1  
2  
3  
4  
5  
6  
7  
8  
9  
10  
11  
12  
13  
14  
15  
16  
17  
18  
19  
20  
21  
22  
23  
24  
25  
26  
27  
28  
29  
30  
31  
32  
33  
34  
35  
36  
37  
38  
39  
40  
41  
42  
43  
44  
45  
46  
47  
48  
49  
50  
51  
52  
53  
54  
55  
56  
57  
58  
59  
60

## Graphical Abstract

